

RSC Advances



This is an *Accepted Manuscript*, which has been through the Royal Society of Chemistry peer review process and has been accepted for publication.

Accepted Manuscripts are published online shortly after acceptance, before technical editing, formatting and proof reading. Using this free service, authors can make their results available to the community, in citable form, before we publish the edited article. This *Accepted Manuscript* will be replaced by the edited, formatted and paginated article as soon as this is available.

You can find more information about *Accepted Manuscripts* in the [Information for Authors](#).

Please note that technical editing may introduce minor changes to the text and/or graphics, which may alter content. The journal's standard [Terms & Conditions](#) and the [Ethical guidelines](#) still apply. In no event shall the Royal Society of Chemistry be held responsible for any errors or omissions in this *Accepted Manuscript* or any consequences arising from the use of any information it contains.

Highly Dispersible Graphene Oxide Reinforced Polypyrrole/Polyvinyl alcohol Blend Nanocomposites with High Dielectric Constant and Low Dielectric Loss

Kalim Deshmukh¹, M. Basheer Ahamed¹, S.K. Khadheer Pasha², Rajendra R. Deshmukh³, Pundlik R. Bhagat⁴

¹Department of Physics, B.S. Abdur Rahman University, Chennai-600048, TN, India

²Sensors Laboratory, School of Advanced Sciences, VIT University, Vellore - 632014, TN, India

³Department of Physics, Institute of Chemical Technology, Matunga, Mumbai-400019, India

⁴Organic Chemistry Division, School of Advanced Sciences, VIT University, Vellore - 632014, TN, India

Corresponding author: Prof. M. Basheer Ahamed*

Email: mbasheerahamed133@gmail.com,

Phone: +919500101398

Abstract

In the present study, we report the fabrication and characterizations of flexible dielectric nanocomposites consisting of water soluble polypyrrole (WPPy)/polyvinyl alcohol (PVA)/graphene oxide (GO) at different GO loadings (0.5 - 3 wt %). The WPPy/PVA/GO nanocomposites were characterized using Fourier transform infrared spectroscopy (FTIR), Raman spectroscopy, UV-vis spectroscopy (UV), X-ray diffraction (XRD), thermogravimetric analysis (TGA), polarized optical microscopy (POM), Scanning electron microscopy (SEM) and atomic force microscopy (AFM). FTIR studies indicate the strong chemical interaction between GO and polymer systems. SEM results confirm that GO was homogeneously dispersed within the polymer matrix. The nanocomposites exhibit significant enhancement in the dielectric constant with low dielectric loss values as a function of GO loading which resulted from the fine dispersion of GO in the polymer matrix. The dielectric constant increases from ($\epsilon = 27.93$, 50 Hz, 150°C) for WPPy/PVA (50/50) blend to ($\epsilon = 155.18$, 50 Hz, 150°C) for nanocomposites with 3 wt % GO loading and the dielectric loss increases from ($\tan \delta = 2.01$, 50 Hz, 150°C) for WPPy/PVA (50/50) blend to ($\tan \delta = 4.71$, 50 Hz, 150°C) for nanocomposites with 3 wt % GO loading. Thus, these high-k WPPy/PVA/GO nanocomposites are potential flexible high-performance dielectric materials for electronic devices such as high-frequency capacitors or embedded capacitors.

Key words: high- k materials, nanocomposites, colloidal processing; dielectric properties

1. Introduction

The development of novel materials for embedded capacitor applications are in great and urgent demand. With the rapid development of electronic industry, extensive research work has been done on the fabrication of electronic devices with enhanced dielectric constant (high-K), excellent mechanical strength and easy processability. Recently, polymer nanocomposites having high dielectric constant (high K), low dielectric loss and easy processability have been in increasing demand due to their important applications in modern nanoelectronics including high speed integrated circuits and high charge storage devices.¹⁻⁶ These materials are widely accepted in telecommunication and electronic industries for their applications as gate dielectrics, single or multi-layer capacitors and as dielectric resonators.^{7, 8} Therefore, much attention has been paid to the development of dielectric polymer composite with high dielectric constant because of their advantages which includes low-cost fabrication process, light weight and good flexibility.^{9, 10} High dielectric constant and low dielectric loss materials are imperative to realise the applications of embedded capacitors which is one of the most important and emerging technologies for electronic packaging. In addition, using a polymer as a matrix allows easy and low-cost processing and one can use processing method such as solution blending, extrusion, hot pressing or moulding very effectively.

Graphene is a rising star of materials community, which consist of a one atom thick two-dimensional honeycomb structure of sp^2 bonded carbon atoms.¹¹ The extraordinary properties of graphene such as high surface area, high flexibility, low mass density, high electrical conductivity, thermal properties and extraordinary mechanical properties makes it suitable candidate for various multi-range technological applications.¹²⁻¹⁴ Graphene is reported to be the strongest material ever tested in the world with the superior mechanical strength of 130 GPa and Young's modulus of 1TPa. Recent studies showed that graphene nanosheets can be considered as better nano filler for the preparation of the polymer nanocomposites because it can provide a combination of extraordinary physical properties. A simple and practical approach has been reported to synthesize graphene reinforced polymer nanocomposites by incorporating graphene oxide (GO) into the polymer matrix which is the most reliable and effective route for the preparation of polymer/graphene nanocomposites.^{15, 16} GO is prepared by intercalation and oxidation of graphite with strong acids which introduces plenty of oxygen-containing functional groups to the graphite layer.¹⁶ The structure of GO consists of various oxygen-containing functional groups which helps in the synthesis of various GO/polymer composites with enhanced properties. To date, various graphene and GO/polymer

nanocomposites have been widely studied including polycarbonate¹⁷, polyimide¹⁸, polystyrene^{16, 19, 20}, polymethylmethacrylate²¹ and so on by colloidal blending and achieved significant reinforcement effect.^{16, 22} The versatility of graphene-based polymer nanocomposites suggests their potential applications in electronics, automotive, aerospace and packaging industry. The fabrication of high-performance graphene-based polymer nanocomposites requires a molecular level dispersion of graphene through the polymer matrix.

Polypyrrole (PPy) is one of the most important and promising intrinsically conducting polymers (ICPs) widely used for multifunctional applications including supercapacitors, electrochromic devices, sensors and antistatic coatings. It belongs to the class of heterocyclic conjugated polymer systems. PPy has been chosen as a polymer matrix owing to its several advantages such as environmental stability, easy to synthesis and high conductivity as compared to other conducting polymers.²³ However, insolubility and poor mechanical strengths are the barriers for the mass production of PPy. One of the possible ways to improve these properties of PPy is to form composites of PPy with other polymer systems having better mechanical and optical properties, good stability and processability. Polyvinyl alcohol (PVA) is a water soluble synthetic polymer having high hydrophilicity and biocompatibility. PVA has been chosen in the present study because of its excellent film-forming ability, chemical stability, emulsifying and adhesive properties.^{24, 25} PVA is one of the most important commodity polymers which have been studied extensively due to its excellent mechanical and thermal properties. Since PVA is a semicrystalline polymer, its important features are the presence of crystalline and amorphous regions. The crystalline region acts as a possible cross-linking point. The interfacial effect between crystalline and amorphous regions, the hydroxyl groups and the hydrogen bonding between them has a great influence on the properties of PVA.²⁶⁻²⁸

In this paper, we report fabrication and characterization of highly dispersible GO reinforced polymer composites consisting of water soluble polypyrrole (WPPy) and PVA. The comprehensive investigations on the structural, morphological, optical, and thermal properties of WPPy/PVA/GO nanocomposites were carried out. The dielectric properties such as dielectric constant and dielectric loss were also measured in order to check the feasibility of nanocomposite for embedded capacitor applications.

2. Experimental details

2.1 Materials used

Polypyrrole aqueous dispersion (WPPy) was supplied by Eeonyx corporation, Ltd., USA. Polyvinyl alcohol of molecular weight 85,000-124,000 g/mol and degree of hydrolysis 87-89% was purchased from Sigma-Aldrich, India. Natural graphite powder with particle size of about 40 μm was supplied by Carbotech Engineers, Jaipur, India. Sulfuric acid (H_2SO_4), potassium permanganate (KMnO_4), sodium nitrate (NaNO_3) and 30% hydrogen peroxide (H_2O_2) were purchased from S.D. Fine Chemicals, Mumbai, India and used without further purifications. Double distilled water was used as a solvent throughout the study.

2.2 Synthesis of Graphene Oxide

GO was synthesized from natural graphite powder using modified Hummers method. In a typical synthesis process, 5 g of graphite powder was added with 150 ml of concentrated H_2SO_4 , to which 3 g of NaNO_3 was subsequently added and mixed well in a 1000 ml round bottom flask. The mixture was kept in an ice bath for 4 h with stirring at temperature 5°C and 9 g of KMnO_4 was gradually added with constant stirring. To avoid sudden increase in temperature, the rate of addition was controlled carefully. The ice bath was then removed and the mixture temperature was maintained at 40°C . After stirring for 2 hours until it became a brown paste, 150 ml of deionized water was added for dilution. Finally, the mixture was stirred at 98°C for about 1 hour until the colour changes from brown to yellow. Subsequently, the mixture was stirred for another 10 min and then diluted by adding 650 ml of deionized water. This was followed by addition of 30 ml of H_2O_2 (30 wt %) to the mixture to reduce residual KMnO_4 . Finally, the solution was then filtered and washed several times with deionized water and dried further at 60°C for 12 h to obtain GO powder. The particle size of the synthesized GO powder was less than 10 μm .

2.3 Synthesis of WPPy/PVA/GO nanocomposites

WPPY/PVA/GO nanocomposites films with different GO loadings (0, 0.5, 1, 1.5, 2, 2.5 and 3 wt %) were prepared by the colloidal processing method. The desired amount of PVA powder was completely dissolved in distilled water at 75°C for 3 hrs. The known quantity of WPPy was added to the solution of PVA and stirred continuously for 4 hrs. GO powder was sonicated in water separately for 30 min. and further added to WPPy/PVA blend solution. The solution so obtained was again stirred overnight before casting it on cleaned glass Petri dish at

60°C for 8 hrs. The WPPy/PVA/GO nanocomposites films of thickness in the range of 40-50 μm were peeled from the glass plate and kept in vacuum desiccators for further study. A schematic representation of the bonding interaction between WPPy, PVA and GO is shown in **Figure 1**. The photographs of different compositions of WPPy/PVA/GO nanocomposites dispersion is shown in **Figure 2**, indicating the formation of a homogeneous dispersion of nanocomposites. The photographs of prepared WPPy/PVA/GO nanocomposites films with different compositions are shown in **Figure 3**. The feed compositions of WPPy/PVA/GO nanocomposites are given in **Table 1**.

3. Characterizations

FTIR spectroscopy of WPPy/PVA/GO nanocomposites was carried out with Fourier Transform Infrared Spectrophotometer (Shimadzu, IRAffinity-1, Japan) in the wavenumber range 400 – 4000 cm^{-1} .

Raman Spectroscopy of Graphite, GO, and WPPy/PVA/GO nanocomposites films was carried out using Raman Scattering Spectrometer (LABRAM HR 800) by using a 633 nm laser and a 1 μm spot size. The samples were exposed for 10 s with a laser power of 10 mW at room temperature in backscattering mode. A charged coupled camera was used to collect the data in the wave number range 1000-3000 cm^{-1} .

UV–vis absorption spectrum of WPPy/PVA/GO dispersion was obtained in the range of 190–600 nm with a Shimadzu UV-2401PC, UV–vis spectrophotometer.

X-ray diffraction patterns of WPPy/PVA/GO nanocomposites films were obtained with a scanning speed and step size of 1°/mm and 0.01° respectively using Bruker AXS D8 focus advanced X-ray diffraction meter (Rigaku, Japan, Tokyo). The scans were taken in the 2 θ range from 5-80° using Cu K α radiation of wavelength $\lambda = 1.54060 \text{ \AA}$.

Thermal stability of WPPy/PVA/GO nanocomposites films was studied using Mettler Toledo, TGA/STDA851, thermogravimetric analyzer operated under N₂ as a purge gas. Samples were heated up to 800°C at a rate of 10°C/min.

The degree of dispersion of WPPy/PVA/GO nanocomposites films was investigated under crossed polarizer at a magnification of 10 X using Olympus Polarizing Optical Microscope (POM), (Olympus BX-53, Singapore).

Microstructure and surface morphology of WPPy/PVA/GO nanocomposites films was examined by scanning electron microscope (Carl Zeiss EVO/18SH, UK). An accelerating voltage of 15 kV was applied to obtain SEM images.

The surface morphology and topography of WPPy/PVA/GO nanocomposites films were studied using tapping mode atomic force microscopy (Nano Surf Easy Scan2, Switzerland), operating in air. For AFM study, samples were prepared by sticking a small piece of composites film on a glass slide.

The dielectric properties of WPPy/PVA/GO nanocomposites films were measured using Wayne Kerr 6500B (Chichester, West Sussex, UK) Precision Impedance Analyzer having an overall frequency range from 20 Hz-20 MHz. In the present investigation, the dielectric properties were investigated in the frequency range from 50 Hz to 20 MHz and temperature in the range 40-150°C with an accuracy of about + 0.1°C.

4. Results and Discussion

4.1 FTIR spectroscopy

FTIR spectroscopy is a widely used technique to study the interaction between molecules. The FTIR spectroscopy was employed to study the structural changes in the WPPy/PVA/GO nanocomposites due to interactions between GO, and polymer systems. The FTIR spectra of GO powder, PVA and WPPy/PVA/GO nanocomposites film is shown in **Figure 3**. The FTIR spectrum in **Figure 3 (a)** shows characteristic peaks of GO. The band at 3441 cm^{-1} is attributed to the O-H stretching vibration and the band at 2920 cm^{-1} is assigned to C-H stretching. The band at 1635 cm^{-1} is attributed to C=C bond of the unoxidized sp^2 group. The band at 1396 cm^{-1} can be assigned to C-O stretching vibration of a carboxylic group and the band at 1116 cm^{-1} can be due to C-O stretching vibrations of an alkoxy group of GO.²⁹⁻³¹ The FTIR spectrum of GO gives evidence of different functional groups (carbonyl, hydroxyl and epoxy) present in the structure of GO. The FTIR spectrum in **Figure 3 (b)** shows various important characteristic peaks of PVA. A strong broadband at 3275 cm^{-1} is assigned to the O-H stretching vibration of the hydroxyl group. The band at 2928 cm^{-1} corresponds to C-H asymmetric stretching vibration of the alkyl group. The band at 1733 cm^{-1} is attributed to the C=O stretching vibration of vinyl acetate group of PVA. Also, the band at 1640 cm^{-1} can be assigned to stretching vibrations of C=O group.²⁴ The band at 1438 cm^{-1} corresponds to CH_2 bending.^{26, 28} The band at 1321 cm^{-1} and 1243 cm^{-1} are corresponding to CH_2 and C-H wagging vibrations respectively. The band at 1084 cm^{-1}

corresponds to the C–O stretching vibration of an acetyl group. The bands observed at 916 and 840 cm^{-1} are attributed to the skeletal vibration of PVA.^{24, 25} The FTIR spectra of WPPy/PVA/GO nanocomposites film with different GO loadings is given in **Figure 3 (c-h)** which shows various FTIR peaks of individual components present in the composites. The broad peak at 3275 cm^{-1} in nanocomposites is due to overlapping of the N-H stretching vibrations of PPy and O-H stretching of absorbed water. The N-H bending vibration of PPy was observed at 1328 cm^{-1} in all the nanocomposites. The WPPy/PVA/GO nanocomposites show a characteristic peak of PPy at 1423 cm^{-1} , which is attributed to C=C stretching of pyrrole ring and the peak at 1045 cm^{-1} which is attributed to C-H in-plane deformation of PPy.³² The peak at 945 cm^{-1} and 1676 cm^{-1} which are attributed to C-H wagging and C=N stretching vibrations of PPy were also observed. The characteristics peak of GO at 1635 cm^{-1} , 1396 cm^{-1} and 1116 cm^{-1} and that of PVA at 1733 cm^{-1} , 916 cm^{-1} and 840 cm^{-1} were also observed in the FTIR spectra of nanocomposites. Thus, FTIR results indicate that the significant interaction has occurred between all the three components of nanocomposites. The presence of oxygen-containing functional groups in the structure of GO has led the successful preparation of nanocomposites.

4.2 Raman Spectroscopy

Raman spectroscopy is strongly sensitive to the electronic structures and very useful technique for characterizations of carbonaceous materials. The Raman spectroscopy is widely used to study the structural integrity of graphite based materials. The Raman spectra of graphite, GO and WPPy/PVA/GO nanocomposites are depicted in **Figure 4**. Graphite (**Figure 4 (a)**) shows a strong G band and a very weak D band, whereas GO shows strong G and D band. As can be seen, graphite shows a prominent G band at 1585 cm^{-1} corresponding to the first order scattering of the E_{2g} mode (E_{2g} phonon of sp^2 carbon atom), 2D band at 2674 cm^{-1} and weak D band at 1326 cm^{-1} corresponding to structural defects and disorders inherent in the graphite (A_{1g} phonons of sp^3 carbon atom).^{33,34} Raman spectrum of GO (**Figure 4 (b)**) shows an intense D band at 1365 cm^{-1} and a G band at 1629 cm^{-1} with D/G intensity ratio of 0.83. The D band at 1365 cm^{-1} of GO indicates that the sp^2 domains are decreased due to extensive oxidation and the G band at 1629 cm^{-1} indicates that the isolated double bonds of GO are resonated slightly as compared to pristine graphite. Thus, harsh chemical oxidation has resulted in significant structural changes in the graphite lattice leading to the formation of different types of oxygen-containing functional groups at the basal plane and at the edges. The Raman spectra of WPPy/PVA/GO nanocomposites is given in **Figure 4 (c-f)** which

show a similar spectrum as GO with a slight shifting of D and G band to 1326 cm^{-1} and 1595 cm^{-1} respectively. These shifts in the Raman bands in WPPy/PVA/GO nanocomposites can be attributed to the restoration of sp^2 hybridized carbon. Such interactions between the filler and the matrix are extremely important for maintaining the adhesion, good mechanical and thermal properties and desirable dielectric properties.

4.3 UV- vis spectroscopy

For preparing nanocomposites by the colloidal blending technique, the distribution of GO in the polymer matrix is largely determined by its dispersion state in the solvent. In the present study, UV- vis spectroscopy studies were carried out to evaluate the dispersibility of GO in the WPPy/PVA matrix. The UV-vis absorbance spectra of WPPy, PVA and GO are shown in **Figure 5(a)**. The UV-vis spectrum of WPPy shows three absorption peaks indicating the existing state of WPPy. A sharp peak at 200 nm, a shoulder at 224 nm and a small peak at 256 nm was observed which are attributed to $\pi\text{-}\pi^*$ transition of the benzenoid ring in the PPy chain. PPy can exist in three different states and these are neutral PPy, polaron (radical cation) and bipolaron (dication). The polaron transitions in PPy can be visible in the region 300-400 nm and bipolaron transitions ($n\text{-}\pi^*$) can be observed in the region 600-900 nm.³⁵ Both these transitions are assigned to the doping level of PPy which represents the protonation stages of PPy chain. Such behaviour of doped PPy causes an easier transition of electrons due to the small energy gap and thus conductivity increases.³⁶ The WPPy used in the present study is the neutral i.e. undoped WPPy because it does not show any UV-visible peaks in the region 300-400 and 600-900 nm. The degree of oxidation and the length of conjugated chain influence the doping level of PPy that in turn affects the absorption spectra.³⁶ The UV-vis spectrum of pristine PVA shows a single peak at 200 nm which could be attributed to the presence of unhydrolyzed acetate group in PVA backbone. Most of the commercially available PVA shows strong absorbance in the region 200-400 nm.³⁷ The UV-vis spectra of GO shows a UV absorption peak at 230 nm which corresponds to $\pi\text{-}\pi^*$ transition of the $\text{C}=\text{C}$ bond. The UV-vis absorbance spectra of WPPy/PVA/GO nanocomposites with different GO loadings are shown in **Figure 5 (b)**. All nanocomposites show a sharp peak around 194 nm and a broad low-intensity peak around 224 nm. Thus the interaction between the functional group of GO and water stabilizes GO in aqueous medium and as the aqueous solutions of polymers are added into the GO dispersion, they disperse

homogeneously and form WPPy/PVA/GO nanocomposites via π - π interaction and Van der Waals forces.

4.5 X-ray diffraction

WPPy/PVA/GO nanocomposites were further characterized using XRD technique to study the structural changes and to evaluate the state of GO dispersion in the polymer matrix. The XRD pattern of graphite powder, GO and PVA is depicted in **Figure 6 (a)**. Graphite powder shows a strong and sharp diffraction peak at $2\theta=26.42^\circ$ which is attributed to high ordered crystalline structure of graphite corresponding to the hexagonal lattice of (002) plane.³⁸ The corresponding interplanar spacing (d) was observed to be 0.33 nm. The XRD pattern of graphite also shows other small peaks at $2\theta=44.12^\circ$ and 54.35° which corresponds to a hexagonal lattice of (100) and (004) respectively. The XRD spectra of GO shows a single characteristic peak at $2\theta = 11.55^\circ$ with an interplanar distance of 0.82 nm. The increased in the interplanar distance is attributed to the intercalation of oxygen, carboxyl and other oxygen containing functional groups.³⁹ This indicates that the oxidation process has disrupted the highly ordered crystalline structure of natural graphite. These results provide evidence that graphite has been converted to graphene oxide. The XRD pattern of pristine PVA shows a crystalline peak at $2\theta = 19.44^\circ$ which can be assigned to (101) reflections, indicating the semi-crystalline nature of PVA having both crystalline and an amorphous structure.²⁴ The crystalline nature of PVA is attributed to the presence of strong inter and intramolecular hydrogen bonding between different monomer units of PVA.^{25,28} The XRD patterns of WPPy/PVA/GO nanocomposites are depicted in **Figure 6 (b)**. The XRD patterns of composites exhibit a broad peak at $2\theta = 19.44^\circ$, which is typical of semicrystalline polymers such as PVA.⁴⁰ Furthermore, the XRD peak of GO ($2\theta = 11.55^\circ$) was not observed in the nanocomposites indicating that the GO was completely exfoliated and most of the GO sheets were dispersed within the polymer matrix.⁴¹

4.6 Thermogravimetric Analysis (TGA)

The thermal stability of graphite, GO and WPPy/PVA/GO nanocomposites was evaluated using thermogravimetric analysis. **Figure 7 (a)** shows TGA thermograms of graphite and GO powders. It can be seen that graphite and GO powder differ in their thermal behaviour, indicating that graphite is thermally more stable than GO. For example, graphite powder does not show any mass loss between room temperature to 600°C , whereas the GO powder showed three major weight loss stages. The first stage of decomposition appears at

the temperature slightly below 100°C and is associated with the evaporation of interlamellar water molecule.⁴² The second stage of decomposition appears in the temperature range 150-250°C which is attributed to the decomposition of CO, CO₂ and some most liable oxygen containing functional groups. The third stage of decomposition appears in the temperature range 250-500°C which is attributed to the decomposition of more stable oxygen containing functional groups such as COOH and –OH.⁴³ Also, GO is thermally stable above 550°C. The thermal stability of PVA, WPPy/PVA blend and WPPy/PVA/GO nanocomposites was also investigated. **Figure 7 (b)** shows the TGA thermograms of PVA and WPPy/PVA blends. PVA shows three stages of weight loss. The initial stage of weight loss appears in the temperature range 70°C- 150°C, which could be due to the elimination of adsorbed water. The second weight loss stage appears in the temperature range 150-300°C which could be attributed to the decomposition of the polymer structure and the final weight loss stage is attributed to the further decomposition of the residue. The TGA thermogram of WPPy/PVA blend shows very less weight loss between room temperature to 450°C and with further increase in temperature the blend samples showed significant weight loss. This indicates that WPPy/PVA blend has better thermal stability as compared to neat PVA which could be due to strong interaction and good compatibility between PVA and WPPy. The TGA thermograms of WPPy/PVA/GO nanocomposites are depicted in **and Figure 7 (c)**. Regardless of GO content, all WPPy/PVA/GO nanocomposites exhibit very similar thermal behaviour. The TGA thermograms of nanocomposites show three stage decomposition processes. The first stage appears at low-temperature range 50-100°C which indicates evaporation of moisture.⁴⁴ The second stage appears in the temperature range 100-300°C which could be due to splitting of polymer main chain. The third step appears in the temperature range 300-450°C which could be attributed to the decomposition of the polymer backbone. Hence, these results indicate that the addition of GO into WPPy/PVA blend matrix did not make any significant contribution to the thermal stability of WPPy/PVA/GO nanocomposites.

4.7 Microscopic Studies

To achieve molecular level dispersion of GO into the polymer matrix is one of the most common challenges because GO was found to agglomerate in polymer matrices. Hence, to generate better results one can use a high energy shear force mixing which creates enough energy to separate agglomeration of GO particles. In the present study, we have used a high energy sonication process which is an effective technique to improve the distribution of GO

particles into the polymer matrix. To understand the dispersion of GO and its reinforcement effect in the polymer matrix, the optical microscopy of WPPy/PVA/GO nanocomposites was carried out and the results are depicted in **Figure 8**. Optical microscopy results provide direct evidence of dispersion quality of the composite films. From **Figure 8**, it can be seen that the homogeneous dispersion of GO in the polymer matrix was achieved. This indicates that GO was homogeneously distributed throughout the polymer matrix. Since GO consist of various hydrophilic groups such as carboxyl and hydroxyl, one may expect the homogeneous dispersion of GO into hydrophilic polymers. The excellent dispersion can be attributed to the improved interfacial adhesion between GO and polymers.

The dispersion of GO and the interfacial effect between the polymer and GO are the two important factors governing the high performance of polymer composites. With this interest, the morphology and microstructure of WPPy/PVA/GO nanocomposites were studied. The SEM images of graphite and GO powder are shown in **Figure 9 (a)**. From SEM image of graphite powder, a flaky shape microstructure, typical of highly crystalline natural graphite can be seen. The SEM image of GO powder also shows flakes like texture reflecting its layered microstructure. The microstructure of WPPy/PVA/GO nanocomposites films are given in **Figure 9 (b)**. It can be seen that GO is clearly well dispersed in the polymer matrix, indicating that most of the graphite sheets are individually exfoliated and dispersed homogeneously into the polymer matrix. Hence, the morphology of WPPy/PVA/GO nanocomposites films suggests that the interfacial interaction between polymer matrices and GO is rather strong which cause flexibility in nanocomposites as compared to pure polymers.

Atomic force microscopy is a powerful technique for the investigation of the morphology and physical properties of nanocomposites. In the present study, AFM was used to quantify the degree of exfoliation of GO and to analyze the distribution of GO in polymer matrices. The surface topography and surface roughness of WPPy/PVA/GO nanocomposites films were studied using tapping mode AFM. Tapping mode AFM can be used to probe surface topology, defects and bending properties of graphene-based materials. The topographic images are depicted in **Figure 10 (a)** and 3D images are depicted in **Figure 10 (b)**. From AFM results, it can be seen that the surface of the composite film became rough after the addition of GO. The surface roughness of the composite drastically increased upon addition of GO which could be due to fine dispersion of GO throughout the polymer matrix. The surface roughness increases from 3.55 nm for 0.5 wt % GO loading to 20.25 nm for 3 wt % GO loading. This observation indicates the strong interfacial interaction between the

constituents of nanocomposites, which can be attributed to the molecular interaction of polar segments of the polymer matrix with rich oxygen-containing functional groups of GO.

4.8 Dielectric Properties

The dielectric properties of polymer nanocomposites are related to the structure-property relationship at the morphological level. The molecular motion or dynamics of nanocomposites in response to various applied fields have a significant effect on the macroscopic properties. Polymer nanocomposites are subjected to ionic, interfacial and dipole polarization upon exposure to an electric field. Polymer nanocomposites with high dielectric constant have various functional applications such as energy storage materials, capacitors, transistors and flexible electronics.⁴⁵⁻⁴⁷ In the present study, the dielectric properties of WPPy/PVA/GO nanocomposite were investigated in the frequency range 50 Hz to 20 MHz and temperature in the range 40-150°C. **Figure 11 (a-f)** shows dielectric constant plots of WPPy/PVA/GO nanocomposites with different wt % of GO loading. It can be seen that the dielectric constant is high at lower frequencies and as the frequency increases, the dielectric constant decreases rapidly. Such frequency dependent behavior of dielectric constant can be well explained by the Maxwell- Wagner effect.⁴⁸ It is worth mentioning that the large surface area of GO provided the strong interfacial polarization at the interface between two phases resulting in the strong interfacial polarization at lower frequencies.⁴⁹ At higher frequencies, the rate of separation of charges is low than the rate of increase of frequency which have a weak influence on the dielectric properties. The maximum value of dielectric constant for WPPy/PVA blend ($\epsilon = 27.93$, 50 Hz, 150°C) was observed. With the incorporation of GO into WPPy/PVA blends, the dielectric constant has increased. All nanocomposites show high values of dielectric constant at lower frequencies. For 0.5 wt % GO loading, the maximum value of dielectric constant ($\epsilon = 48.07$, 50 Hz, 150°C) and for 3 wt % GO loading ($\epsilon = 155.18$, 50 Hz, 150°C) was observed. The comparative data of dielectric constant and dielectric loss of all nanocomposites is given in **Table 2**. Comparing with WPPy/PVA blends, five times increase in dielectric constant was observed for WPPy/PVA/GO nanocomposites with 3 wt % GO loading. Such enhancement in the dielectric constant values indicates that GO was homogeneously dispersed into the polymer matrix and there exist a strong interfacial adhesion between GO and polymers.

Figure 12 (a-f) shows dielectric loss ($\tan \delta$) plots of WPPy/PVA/GO nanocomposites with different wt % of GO loading in the frequency range 50 Hz to 20 MHz and temperature

in the range 40-150°C. As can be seen, the dielectric loss increases as GO loading increases. Also, the values of dielectric loss are high at lower frequencies as compared to higher frequencies. It is mainly due to interfacial polarization relaxation in the composites. The dielectric loss increases from ($\tan \delta = 2.01$, 50 Hz, 150°C) for WPPy/PVA (50/50) blend to ($\tan \delta = 4.71$, 50 Hz, 150°C) for WPPy/PVA/GO nanocomposites with 3 wt % GO loading. The increment in the dielectric properties of WPPy/PVA/GO nanocomposites is attributed to the good compatibility between GO and polymer matrices which arises due to the presence of oxygen-containing functional groups and high surface area of GO. Such nanocomposites, having high dielectric constant with low dielectric loss are attractive as potential materials for various functional applications which include high charge storage capacitors, gate dielectrics and embedded capacitors.^{3, 10, 50} All the above results confirm that the WPPy/PVA/GO nanocomposites are very promising high-k dielectric materials which can be used for high-frequency capacitors or embedded capacitors applications.

5. Conclusions

In summary, a series of WPPy/PVA/GO nanocomposites with different GO contents were prepared by colloidal blending technique. The synthesized GO shows good compatibility between WPPy and PVA matrix due to the presence of a highly hydrophilic oxygen containing functional groups of GO. Raman and FTIR spectroscopy confirms that the preparation of GO from graphite was successful. The morphological studies substantiate the homogeneous dispersion of GO into the polymer matrix. The dielectric property investigations revealed that the different wt % of GO loading into polymer matrix plays a significant role in determining the frequency dependence of dielectric composites. The dielectric constant increases as a function of frequency from ($\epsilon = 27.93$, 50 Hz, 150°C) for WPPy/PVA (50/50) blend to ($\epsilon = 155.18$, 50 Hz, 150°C) for nanocomposites with 3 wt % GO loading. The dielectric loss increases from ($\tan \delta = 2.01$, 50 Hz, 150°C) for WPPy/PVA (50/50) blend to ($\tan \delta = 4.71$, 50 Hz, 150°C) for nanocomposites with 3 wt % GO loading. Thus, it can be concluded that the improvement in the properties of WPPy/PVA/GO nanocomposites can be ascribed to the good dispersion of GO into the polymer matrix and strong interfacial adhesion between them. These high-k, flexible nanocomposites are promising candidate as a flexible dielectric material for high-frequency capacitors or embedded capacitors.

References

1. Y. C. Li, S. C. Tjong, R.K.Y. Li, *Exp. Polym. Lett.* 2011, **5**, 526-534.
2. Y. Rao, S. Ogitali, P. Kohl, C.P. Wong, *J. Appl. Polym. Sci.* 2002, **83**, 1084-1090.
3. Q. M. Zhang, H. Li, M. Poh, C. Huang, *Nature* 2002, **419**, 284-287.
4. Y. Zhang, Y. Wang, M. Li, J. Bai, *ACS Appl. Mater. Interfaces* 2012, **4**, 65-68.
5. Y. Shen, Y. Lin, M. Li, C.W. Nan, *Adv. Mater.* 2007, **19**, 1418-1422.
6. C. Huang, Q.M. Zhang, J. Su, *Appl. Phys. Lett.* 2003, **82**, 3502-3504.
7. P. Barber, S. Balasubramanian, Y. Anguchamy, S. Gong, A. Wibowo, H. Gao, H. Ploehn, H.C. Zur Loye, *Materials*, 2009, **2**, 1697-1733.
8. M. T. Sebastian, H. Jantunen, *Int.J. Appl. Ceram. Technol.* 2010, **7**, 415-434.
9. Y. Li, X. Huang, Z. Hu, P. Jiang, S. Li, T. Tanaka, *ACS Appl. Mater. Interfaces*, 2011, **3**, 4396-4403.
10. Y. Bai, Z.Y. Cheng, V. Bharti, H.S. Xu, Q. M. Zhang, *Appl. Phys. Lett.* 2000, **76**, 3804-3806.
11. A. K. Geim, K.S. Novoslov, *Nat. Mater.* 2007, **6**, 1831-1891.
12. A. N. Grigorenko, M. Polini, K.S. Novoselov, *Nature*, 2012, **6**, 749-758.
13. A. A. Balandin, *Nature*, 2011, **10**, 269-281.
14. C. Lee, J. W. Kysar, J. Hone, X. Wei, *Science*, 2008, **321**, 385-388.
15. S. Park, R.S. Ruoff, *Nat. Immunology*, 2009, **4**, 217-224.
16. H. Kim, A. A. Abdala, C. W. Macosko, *Macromolecules*, 2010, **43**, 6515-6530.
17. O. C. Compton, S. Kim, C. Pierre, J. M. Torkelson, S. T. Nguyen, *Adv. Mater.* 2010, **22**, 4759-4763.
18. A. L. Higginbotham, J. R. Lomeda, A.B. Morgan, J. M. Tour, *ACS Appl. Mater. Interfaces* 2009, **1**, 2256-2261.
19. S. Stankovich, D. A. Dikin, G.H.B. Dommett, K.M. Kohlhaas, E.J. Zimney, E.A. Stach, R.D. Piner, S.T. Nguyen, R.S. Ruoff, *Nature*, 2006, **442**, 282-286.
20. M. Fang, K. G. Wang, H. B. Lu, Y.L. Yang, S. Nutt, *J. Mater. Chem.* 2009, **19**, 7098-7105.
21. D. Chen, H. Zhu, T. Liu, *ACS Appl. Mater. Interf.* 2010, **2**, 3702-3708.
22. J. R. Potts, D.R. Dreyer, C.W. Bielawski, R.S. Ruoff, *Polymer*, 2011, **52**, 5-25.
23. E. Benseddik, M. Makhlonki, J.C. Bernede, S. Lefrant, A. Pron, *Synthetic Metals*, 1995, **72**, 237-242.
24. S. M. Pawde, K. Deshmukh, S. Parab, *J. Appl. Polym. Sci.* 2008, **109**, 1328-1337.

25. S. M. Pawde, K. Deshmukh, *J. Appl. Polym. Sci.* 2008, **109**, 3431-3437.
26. J. Ahmad, K. Deshmukh, M.B. Hagg, *Int. J. Polym. Anal. Charac.* 2013, **18**, 287-296.
27. K. Deshmukh, J. Ahmad, M.B. Hagg, *Ionics*, 2014, **20**, 957-967.
28. J. Ahmad, K. Deshmukh, M. Habib, M.B. Hagg, *Arab. J. Sci. Eng.* 2014, **39**, 6805-6814.
29. V. Eswaraiyah, S.S.J. Aravind, S. Ramprabhu, *J. Mater. Chem.* 2011, **11**, 6800-6803.
30. P. Manivel, S. Ramakrishna, N. K. Kothurkar, N. Ponpandian, D. Mangalaraj, C. Viswanathan, *J. Exp. Nanosci.* 2013, **8**, 311-319.
31. K. Zhang, L.L. Zhang, X.S. Zhao, J. Wu, *Chem. Mater.* 2010, **22**, 1392-1401.
32. N. Su, H. B. Li, S.J. Yuan, S. P. Yi, E. Q. Yin, *Exp. Polym. Lett.* 2012, **6**, 697-705.
33. D. Graf, F. Molitor, K. Ensslin, C. Stampfer, A. Jungen, C. Hierold, L. Wirtz, *Nano Lett.* 2007, **7**, 238-242.
34. M. Fang, J. Long, W. Zhao, L. Wang, G. Chen, *Langmuir*, 2010, **26**, 16771-16774.
35. B. R. Saunders, K. S. Murray, R. J. Fleming, D.G. McCulloch, L. J. Brown, J. D. Cashion, *Chem. Mat.* 1994, **6**, 697-706.
36. Y. Shen, M. Wan, *Synth. Met.* 1998, **96**, 127-132.
37. H. M. Zidan, *Polym. Test.* 1999, **18**, 449-461.
38. A. B. Bourlinos, D. Gournis, D. Petridis, T. Szabo, A. Szeri, I. Dekany, *Langmuir*, 2003, **19**, 6050-6055.
39. R. Koizhaiganova, H. J. Kim, T. Vasudevan, S. Kudaibergenov, M. S. Lee, *J. Appl. Polym. Sci.* 2010, **115**, 2448-2454.
40. M. Alkan, R. Benlikaya, *J. Appl. Polym. Sci.* 2009, **112**, 3764-3774.
41. T. Kuilla, S. Bhadra, D. Yao, N. H. Kim, S. Bose, J. H. Lee, 2010, **35**, 1350-1375.
42. Y. Zhang, H. Ma, Q. Zhang, J. Peng, J. Li, M. Zhai, Z. Yu, *J. Mater. Chem.* 2012, **22**, 13064-13069.
43. P. Zou, H. Feng, Z. Xu, L. Zhang, Y. Zhang, W. Xia, W. Zhang, *Chem. Cent. J.* 2013, **7**, 39-49.
44. J. Zhang, J. Qiao, G. Jiang, L. Liu, Y. Liu, *J. Power Sources*, 2013, **240**, 359-367.
45. L. J. Ramasanta, M. Hernandez, M. A. Lopez-Manchaob, R. Verdejo, *Nanoscale. Res. Lett.* 2011, **6**, 508-513.
46. P. Brochu, Q. Pei, *Macromol. Rapid Commun.* 2010, **31**, 10-36.
47. R. Li, C. Xiong, D. Kuang, L. Dong, Y. Lei, J. Yao, M. Jiang, L. Li, *Macromol. Rapid Commun.* 2008, **29**, 1449-1454.
48. Y. C. Li, S.C. Li, R.K.Y. Tjong, *Synth. Met.* 2010, **160**, 1912-1919.

49. B. H. Fan, J.W. Zha, D. Wang, J. Zhao, Z.M. Dang, Appl. Phys. Lett. 2012, **100**, 0129030-012903.
50. A. Facchetti, M.H. Yoon, T. J. Marks, Adv. Mater. 2005, **17**, 1705-1725.

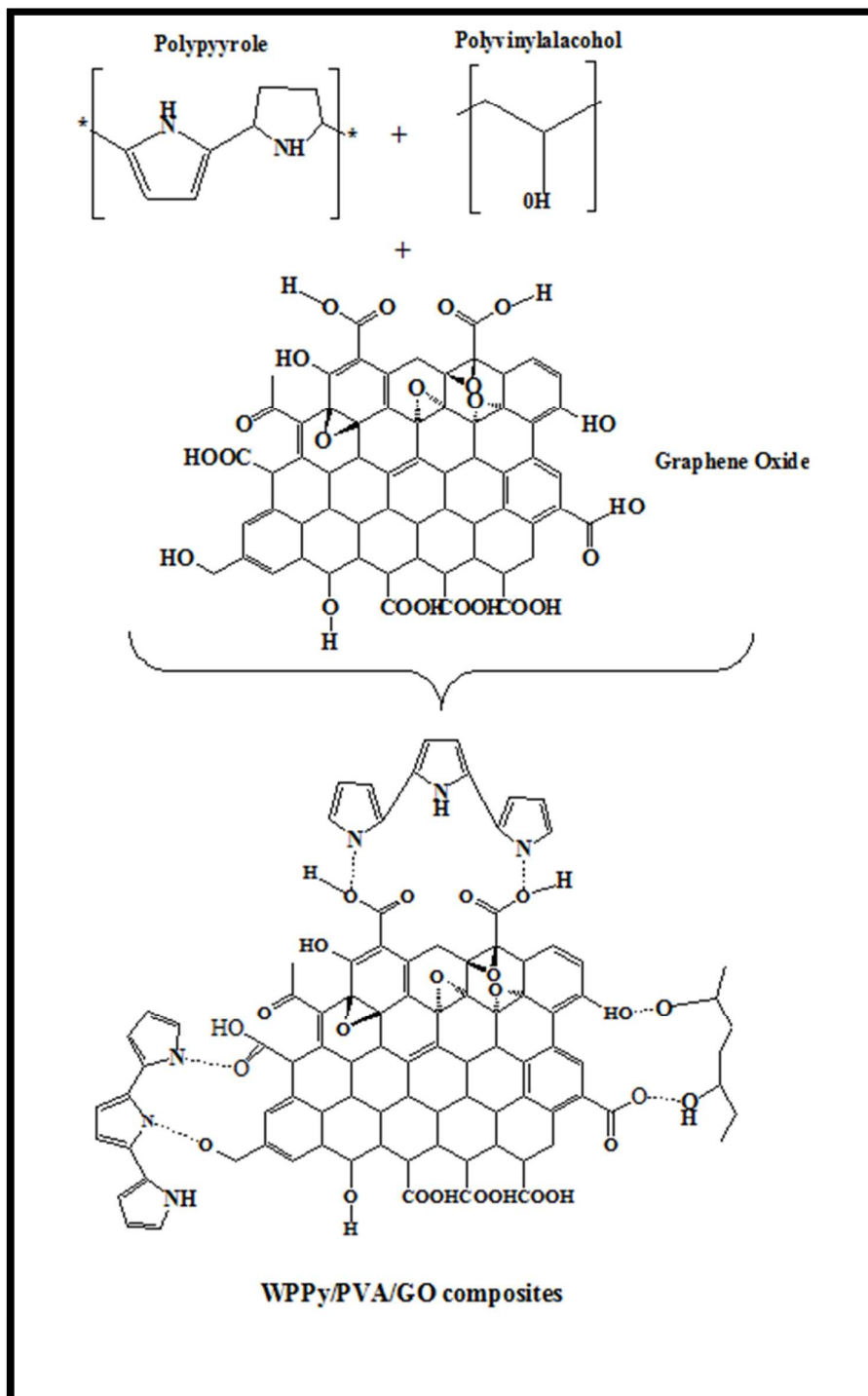
Figures and Tables

Figure 1: Schematic representation of the bonding interaction between WPPy, PVA and GO.

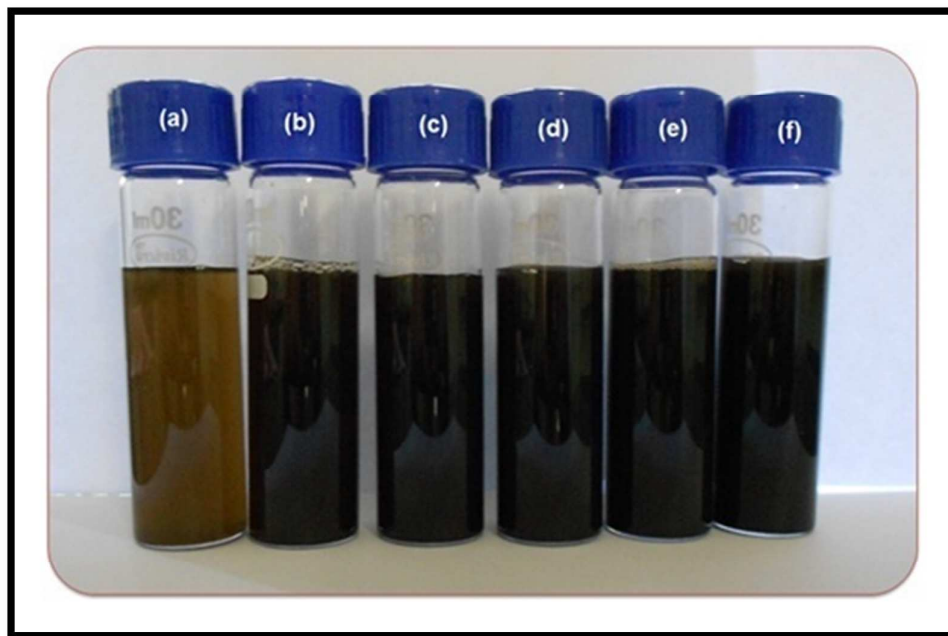


Figure 2 (a): Photographs showing WPPy/PVA/GO dispersion having different GO loadings (a) 0.5 wt % GO (b) 1 wt % GO (c) 1.5 wt % GO (d) 2 wt % GO (e) 2.5 wt % GO (f) 3 wt % GO

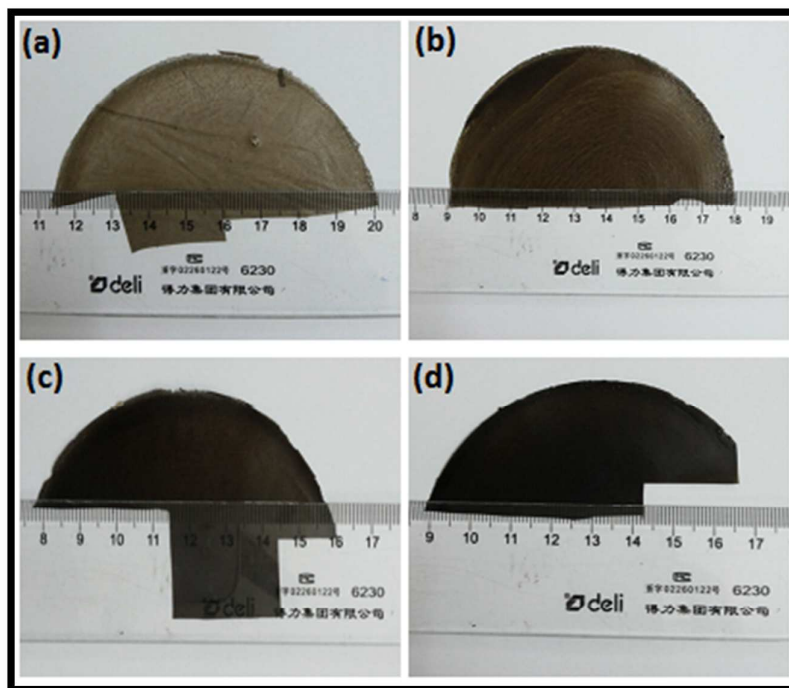


Figure 2 (b): Photographs of WPPy/PVA/GO composite films (a) 0.5 wt % GO (b) 1 wt % GO (c) 2 wt % GO (d) 3 wt % GO loadings

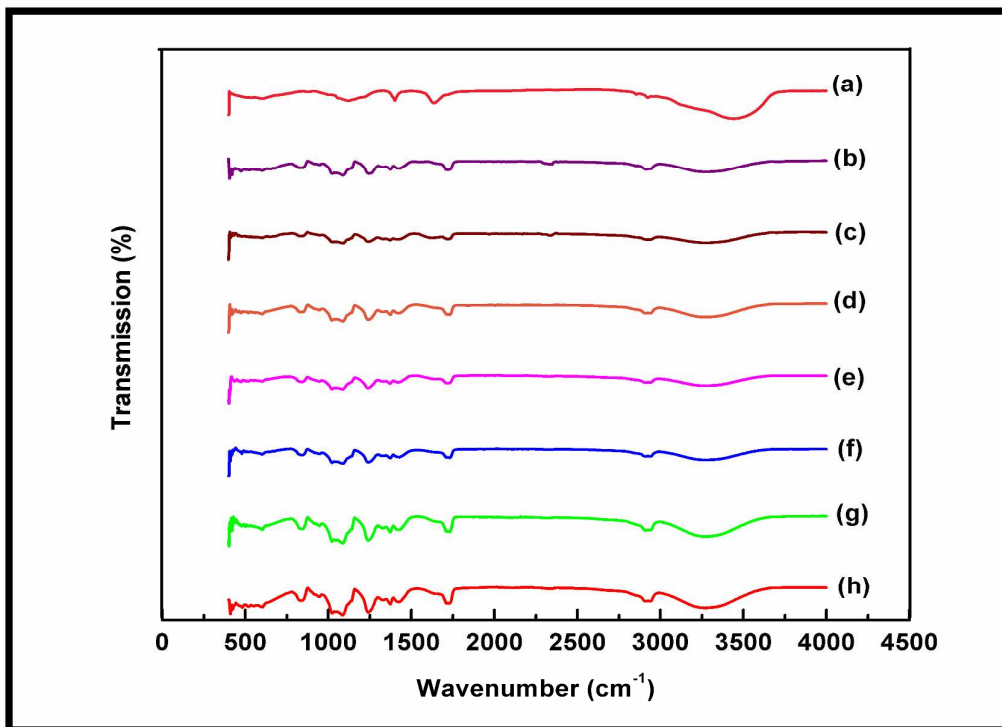


Figure 3: FTIR spectra of WPPy/PVA/GO composite films (a) GO powder (b) PVA (c) 0.5 wt % GO (d) 1 wt % GO (e) 1.5 wt % GO (f) 2 wt % GO (g) 2.5 wt % (h) 3 wt % GO

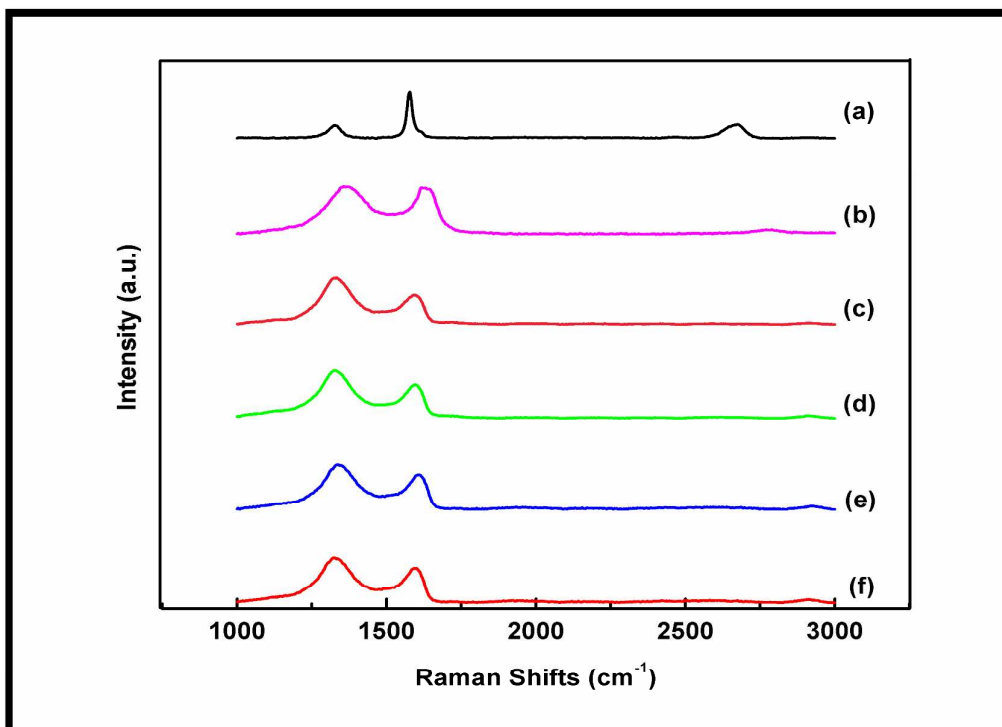


Figure 4: Raman spectra of Graphite, GO and WPPy/PVA/GO composite films. (a) Graphite (b) GO (c) 0.5 wt % GO (d) 1.5 wt % GO (e) 2.5 wt % GO (f) 3 wt % GO

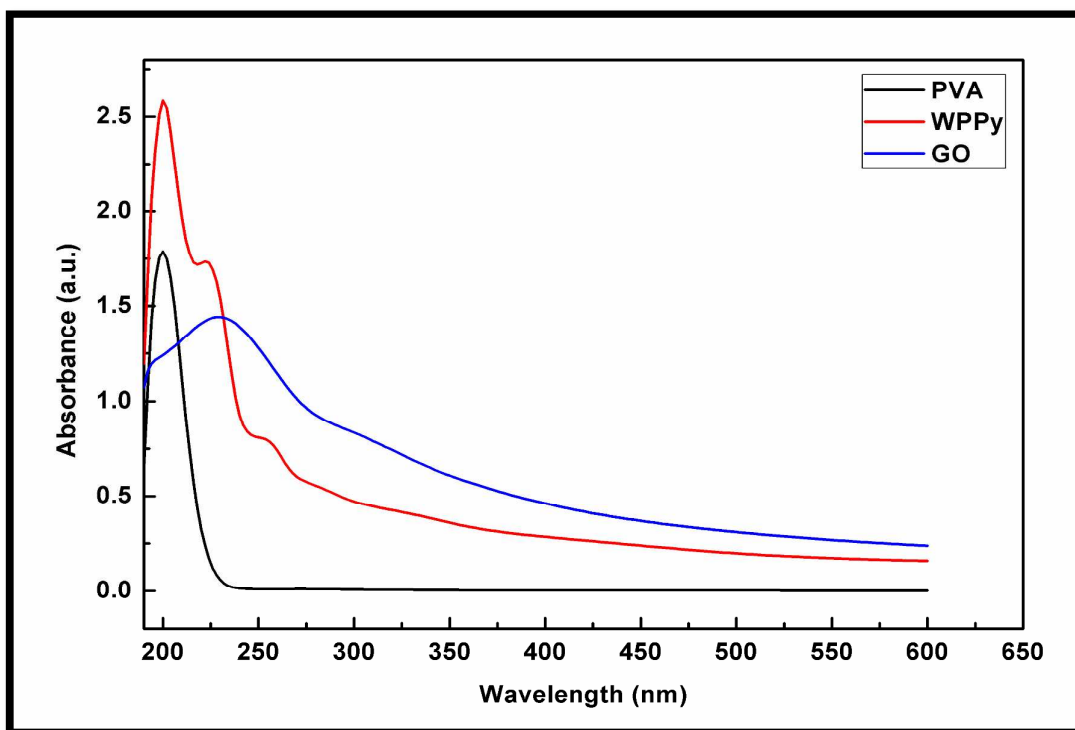


Figure 5 (a): UV-vis spectra of PVA, WPPy and GO solution.

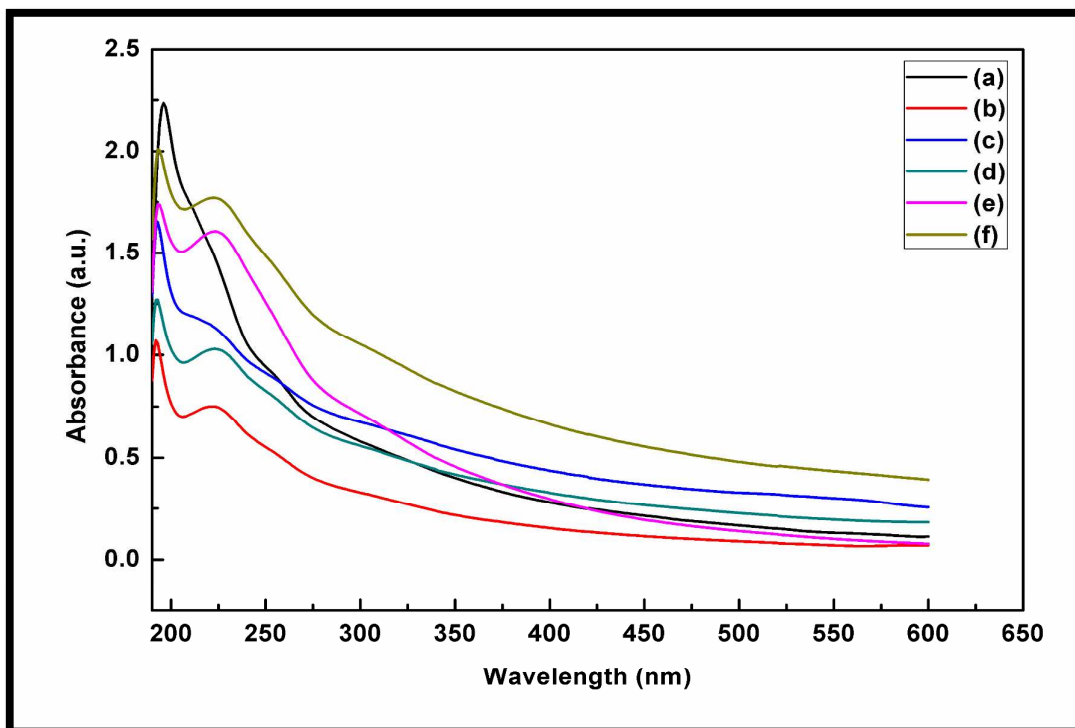


Figure 5 (b): UV-vis spectra of WPPy/PVA/GO composites (a) 0.5 wt% GO (b) 1 wt% GO (c) 1.5 wt% GO (d) 2 wt% GO (e) 2.5 wt % GO (f) 3 wt % GO

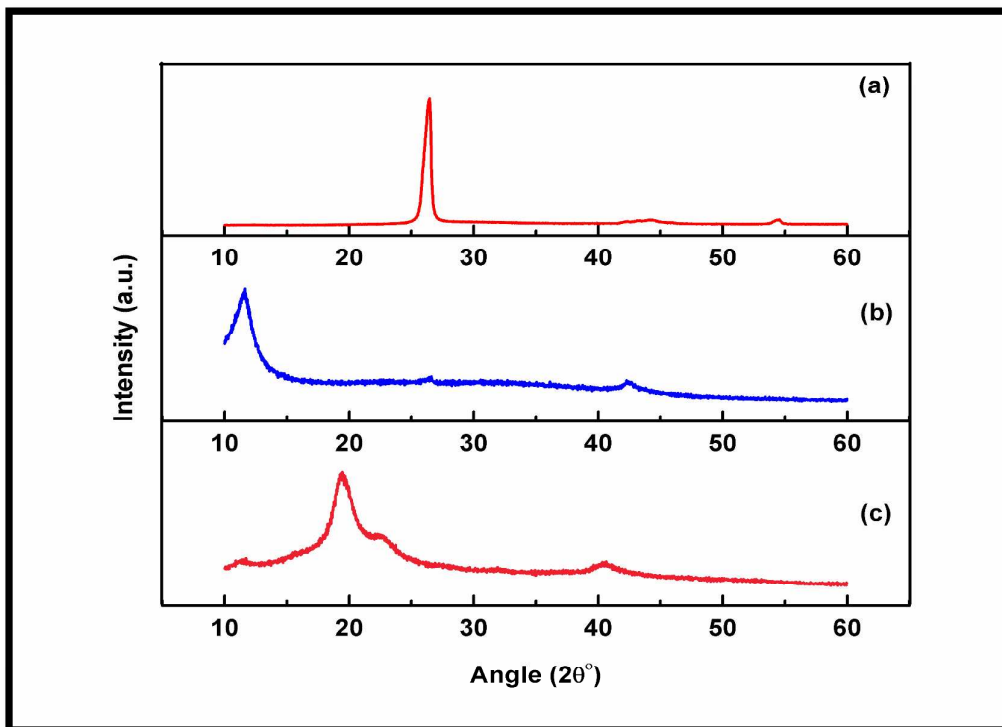


Figure 6 (a): XRD spectra of (a) Graphite powder (b) GO powder (c) PVA

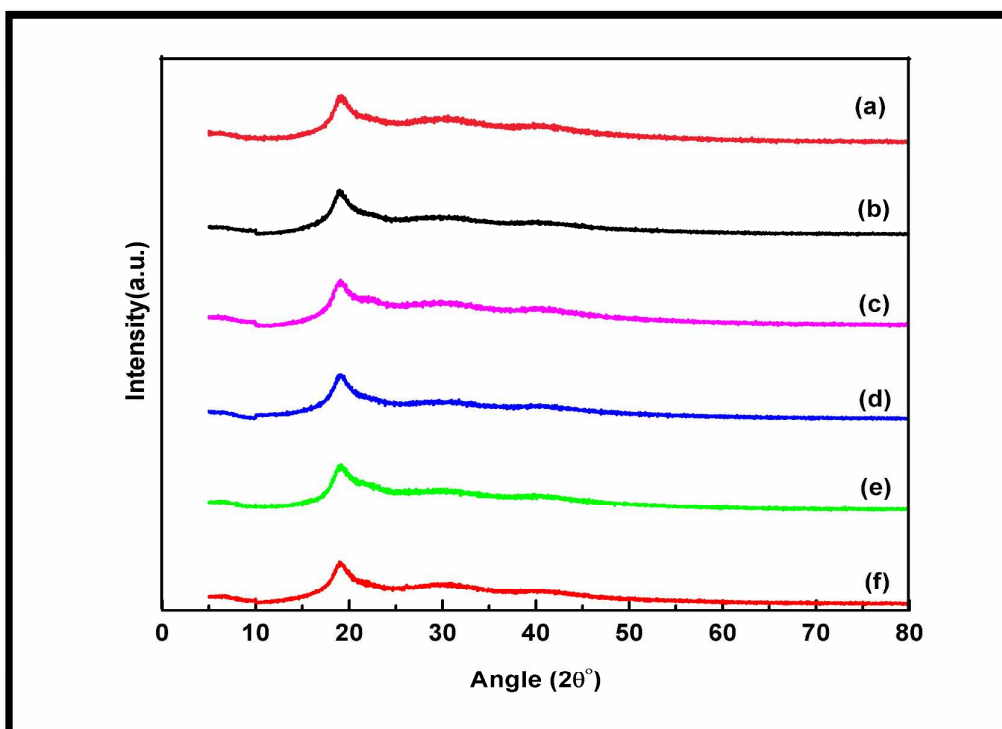


Figure 6 (b): XRD spectra of WPPy/PVA/GO composites (a) 0.5 wt% GO (b) 1 wt% GO (c) 1.5 wt% GO (d) 2 wt% GO (e) 2.5 wt% GO (f) 3 wt % GO

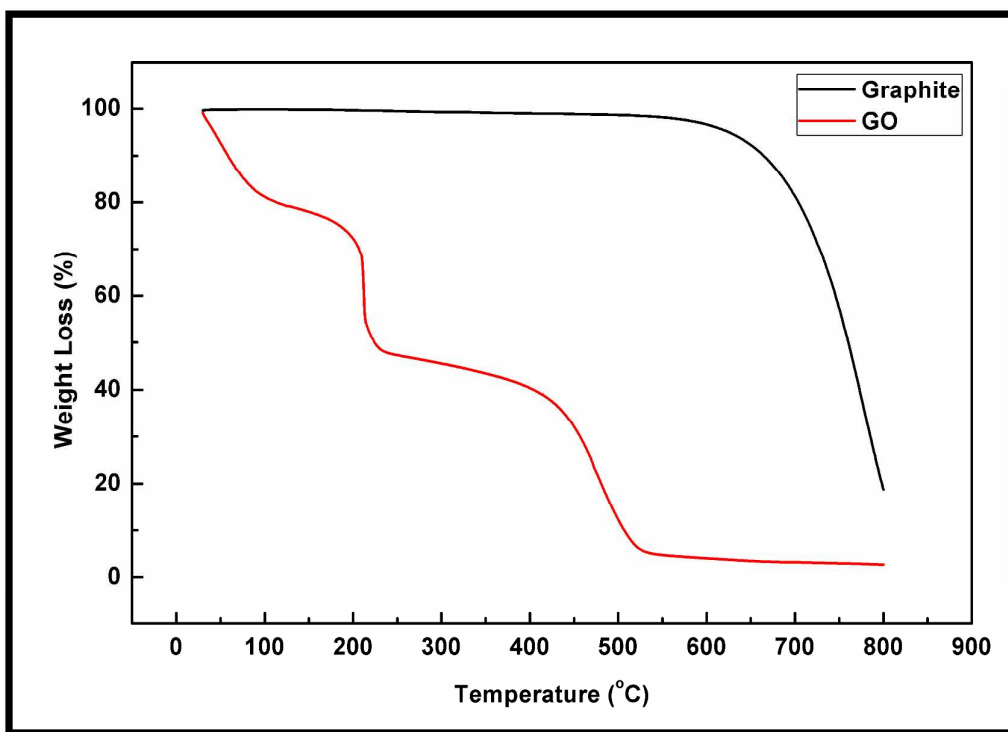


Figure 7 (a): TGA thermograms of graphite and GO powders.

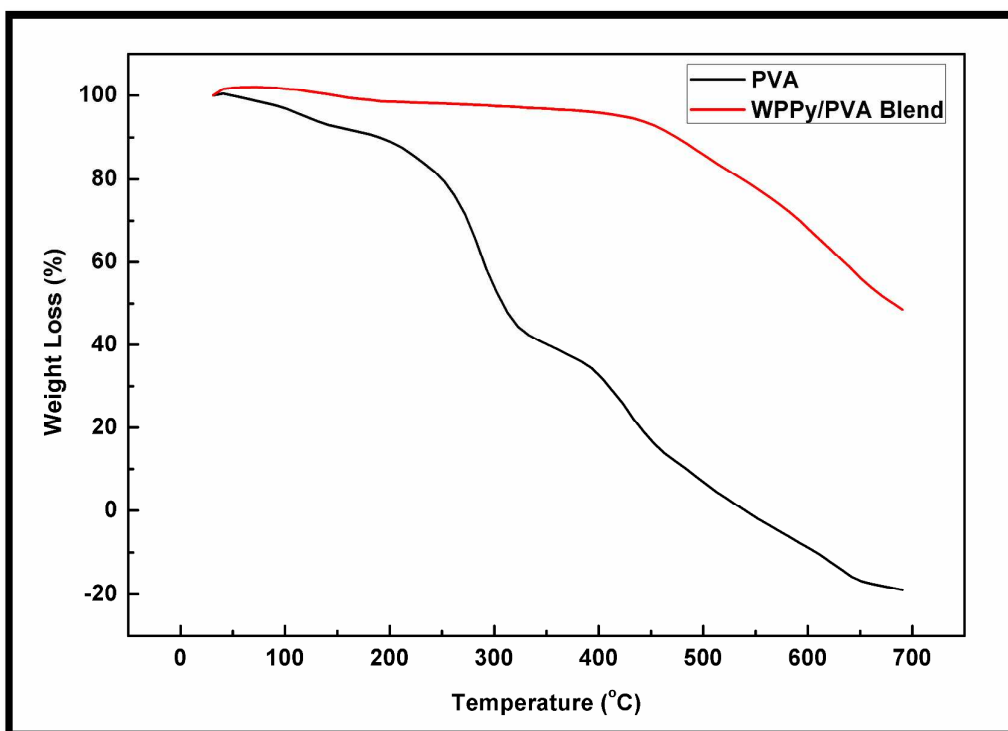


Figure 7 (b): TGA thermograms of PVA and WPPy/PVA (50/50) blends.

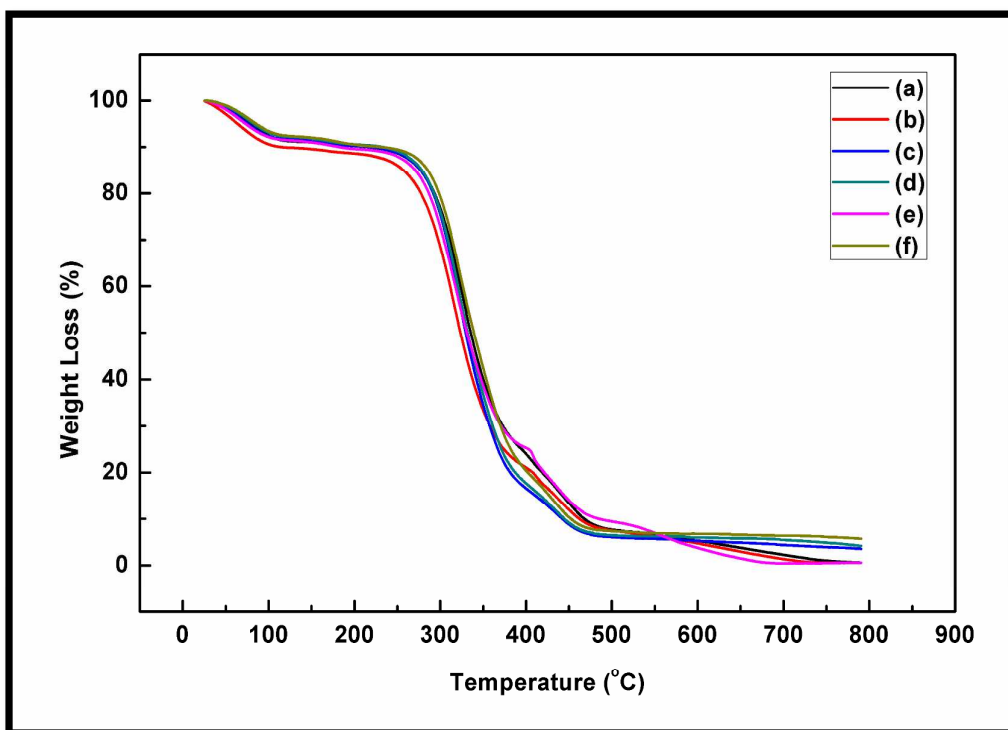


Figure 7 (c): TGA thermograms of WPPy/PVA/GO composites (a) 0.5 wt% GO (b) 1 wt% GO (c) 1.5 wt% GO (d) 2 wt% GO (e) 2.5 wt% GO (f) 3 wt% GO.

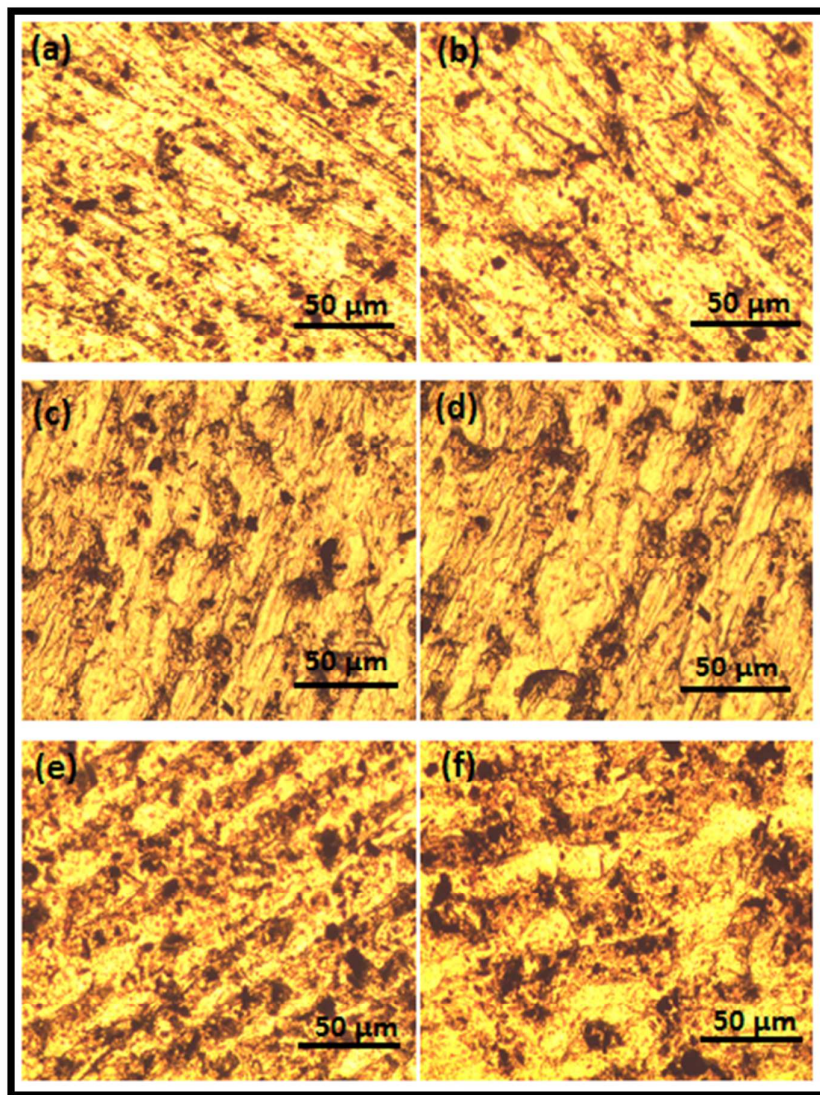


Figure 8: Optical microscopy images of WPPy/PVA/GO composites (a) 0.5 wt% GO (b) 1 wt% GO (c) 1.5 wt% GO (d) 2 wt% GO (e) 2.5 wt% GO (f) 3 wt% GO.

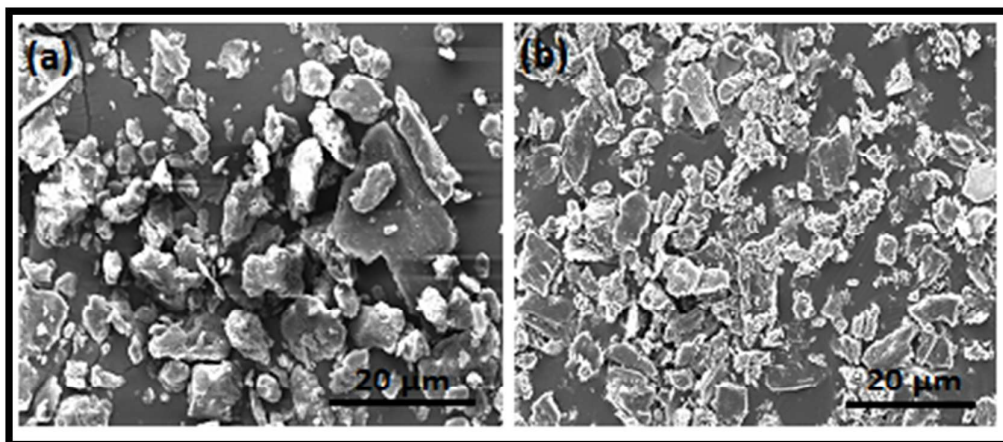


Figure 9 (a): SEM micrographs of (a) graphite powder (b) GO powder

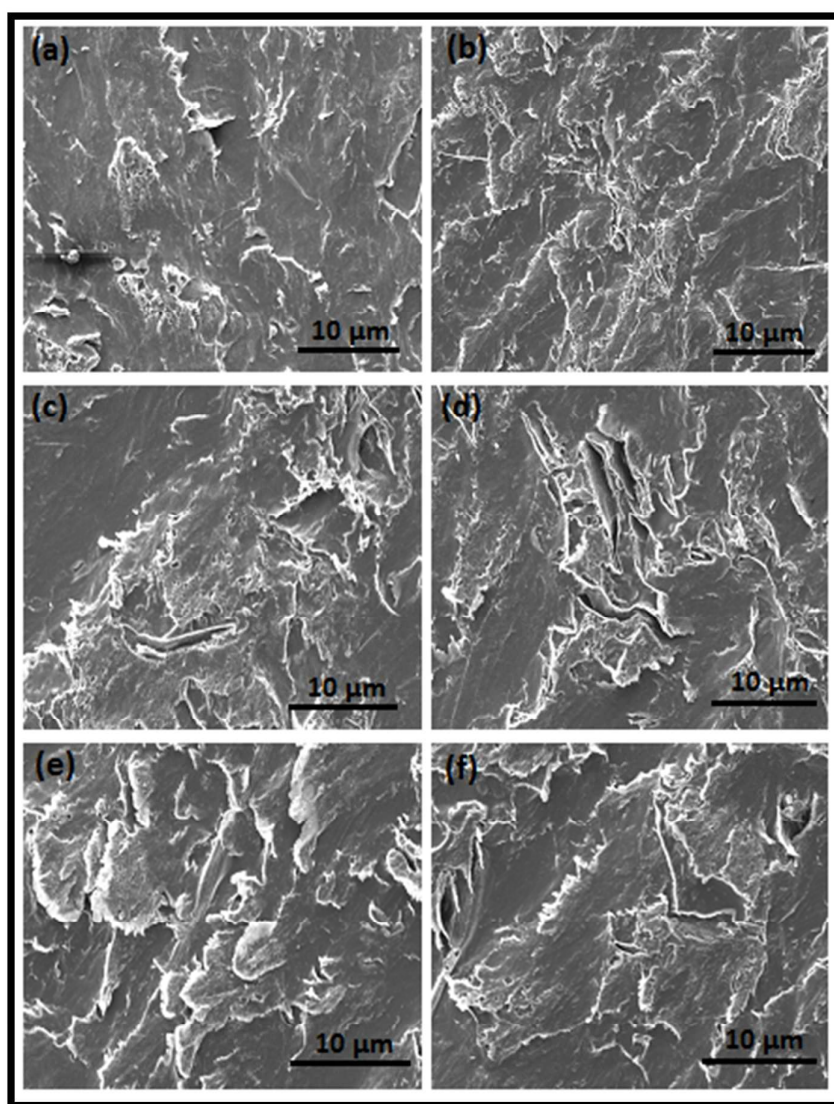


Figure 9 (b): SEM micrographs of WPPy/PVA/GO composites (a) 0.5 wt% GO (b) 1 wt% GO (c) 1.5 wt% GO (d) 2 wt% GO (e) 2.5 wt% GO (f) 3 wt% GO.

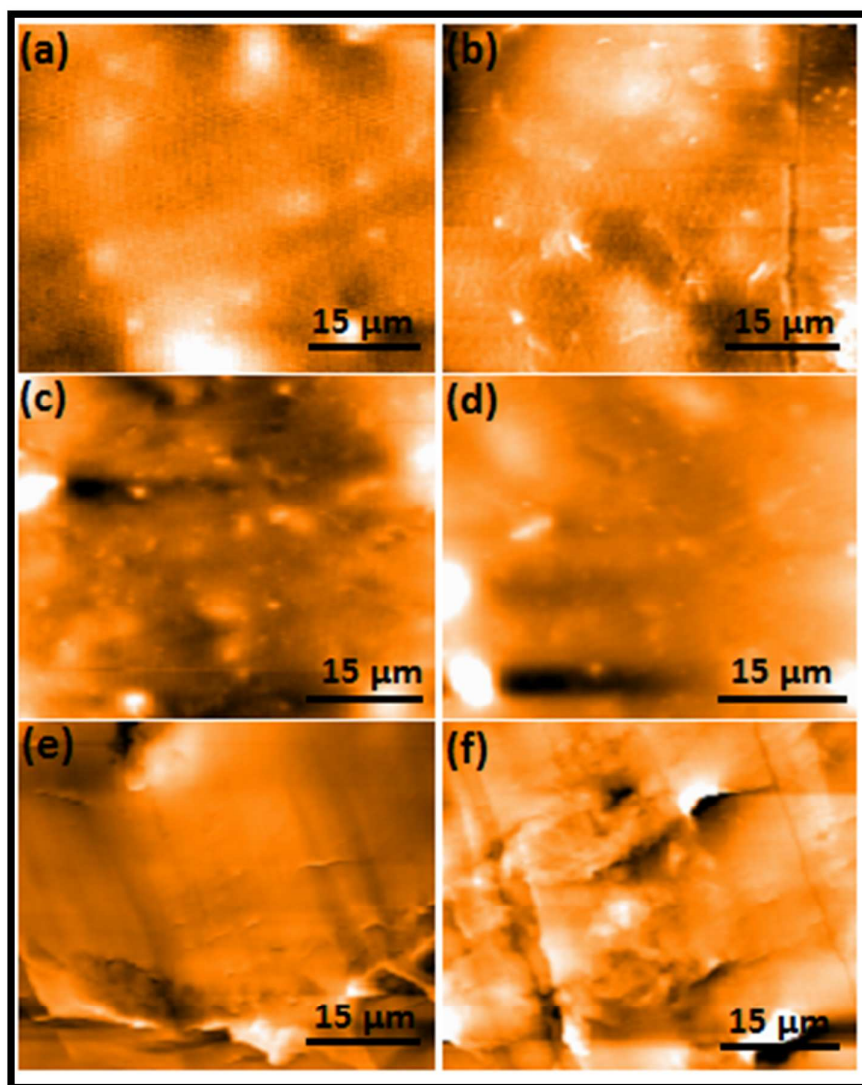


Figure 10 (a): AFM topographic images of WPPy/PVA/GO composites (a) 0.5 wt% GO (b) 1 wt% GO (c) 1.5 wt% GO (d) 2 wt% GO (e) 2.5 wt% GO (f) 3 wt% GO.

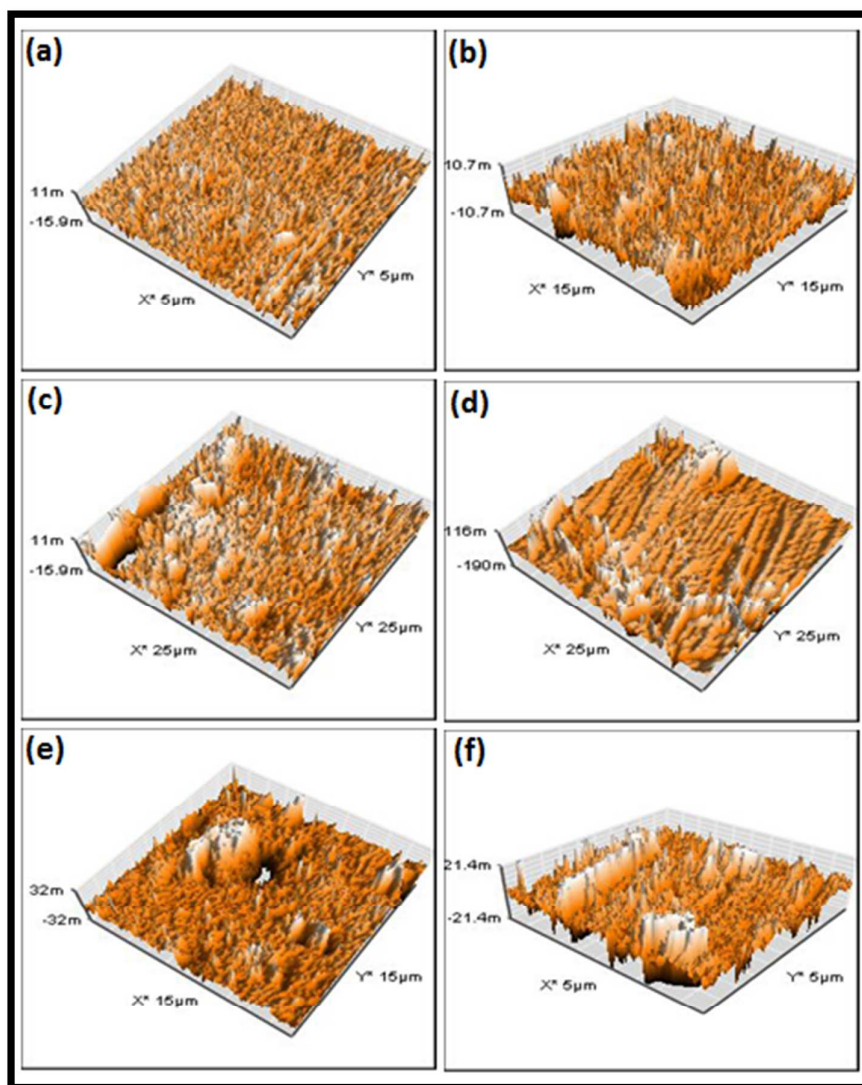


Figure 10 (b): AFM 3D images of WPPy/PVA/GO composites (a) 0.5 wt% GO (b) 1 wt% GO (c) 1.5 wt% GO (d) 2 wt% GO (e) 2.5 wt% GO (f) 3 wt% GO.

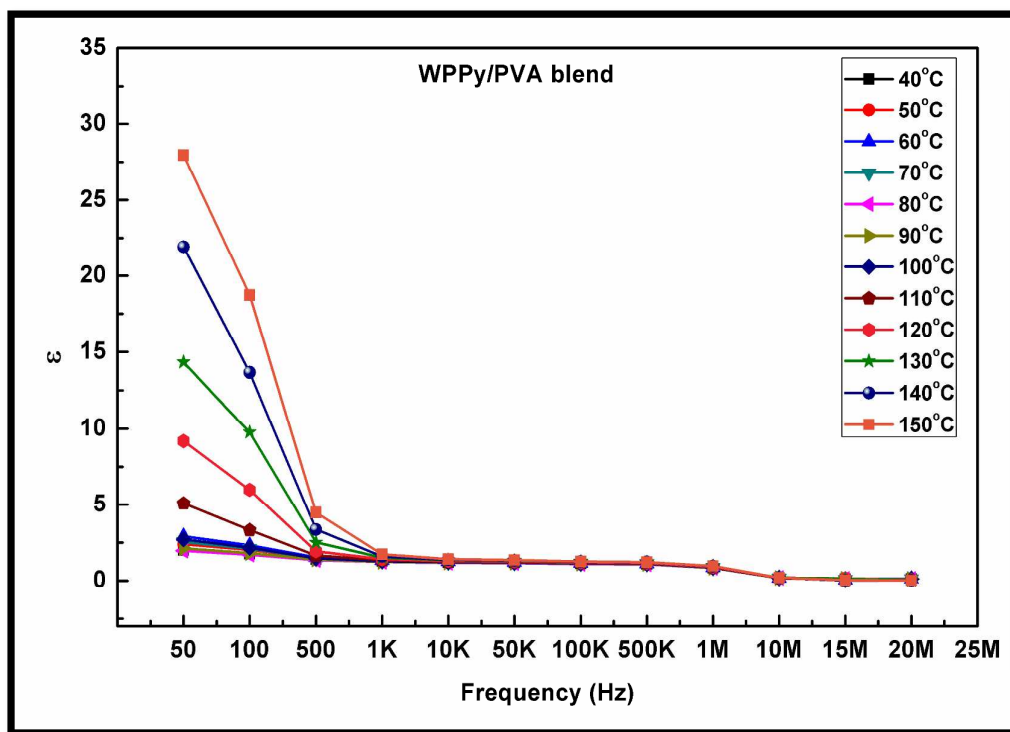


Figure 11 (a): Dielectric constants of WPPy/PVA (50/50) blend as a function of frequency at various temperatures.

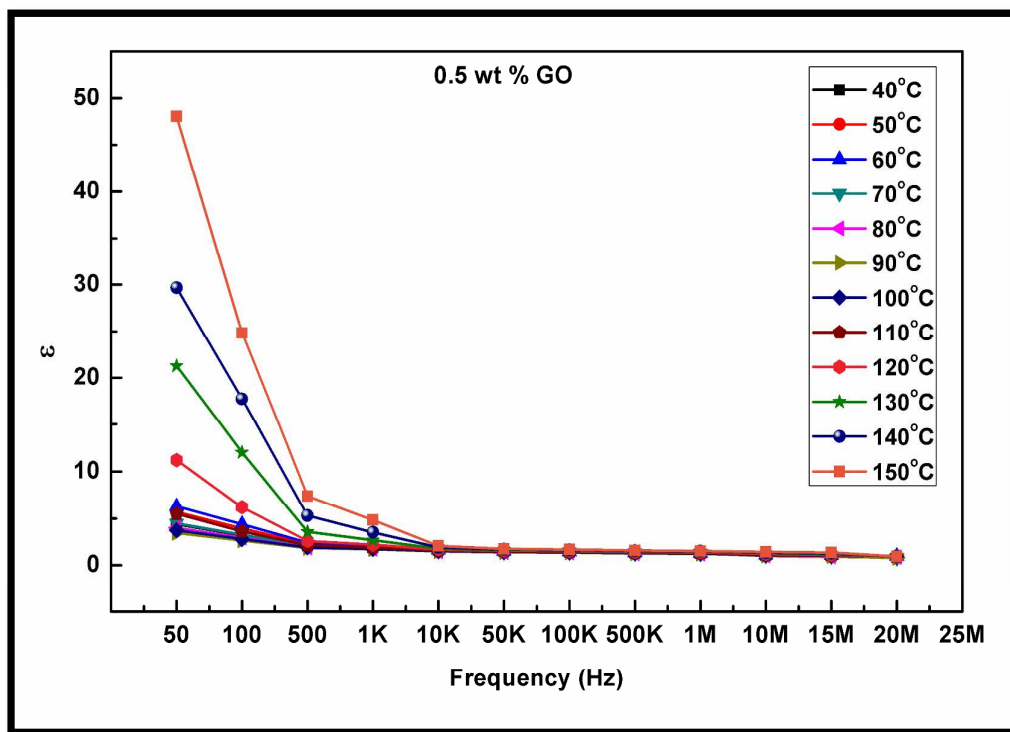


Figure 11 (b): Dielectric constants of WPPy/PVA/GO composite with 0.5 wt% GO loading as a function of frequency at various temperatures.

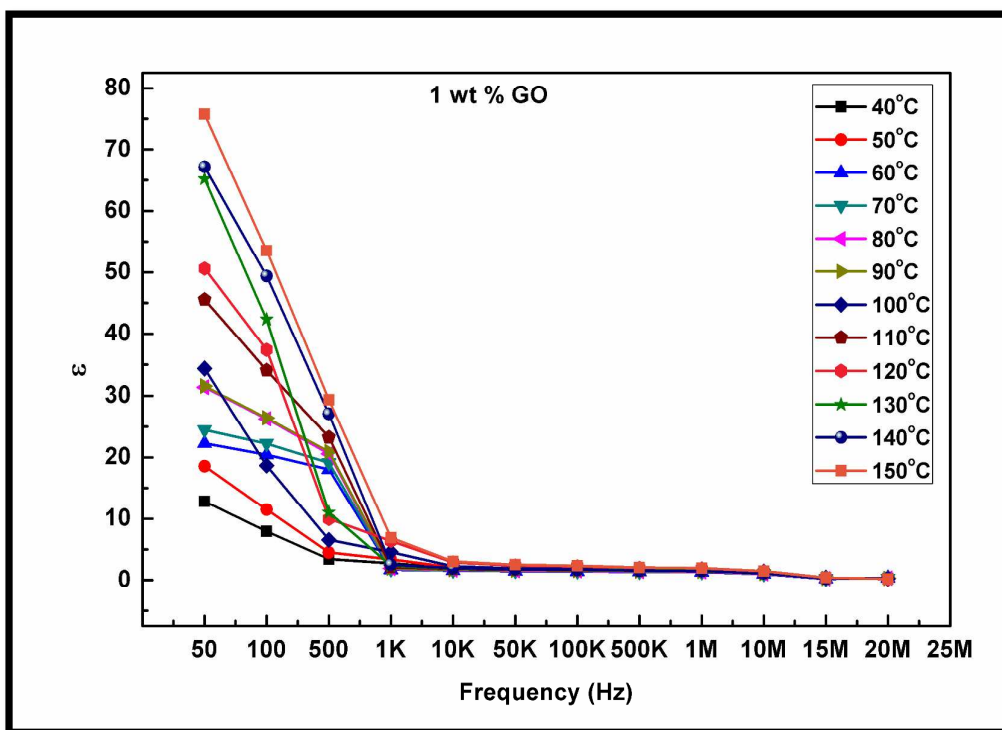


Figure 11 (c): Dielectric constants of WPPy/PVA/GO composite with 1 wt% GO loading as a function of frequency at various temperatures.

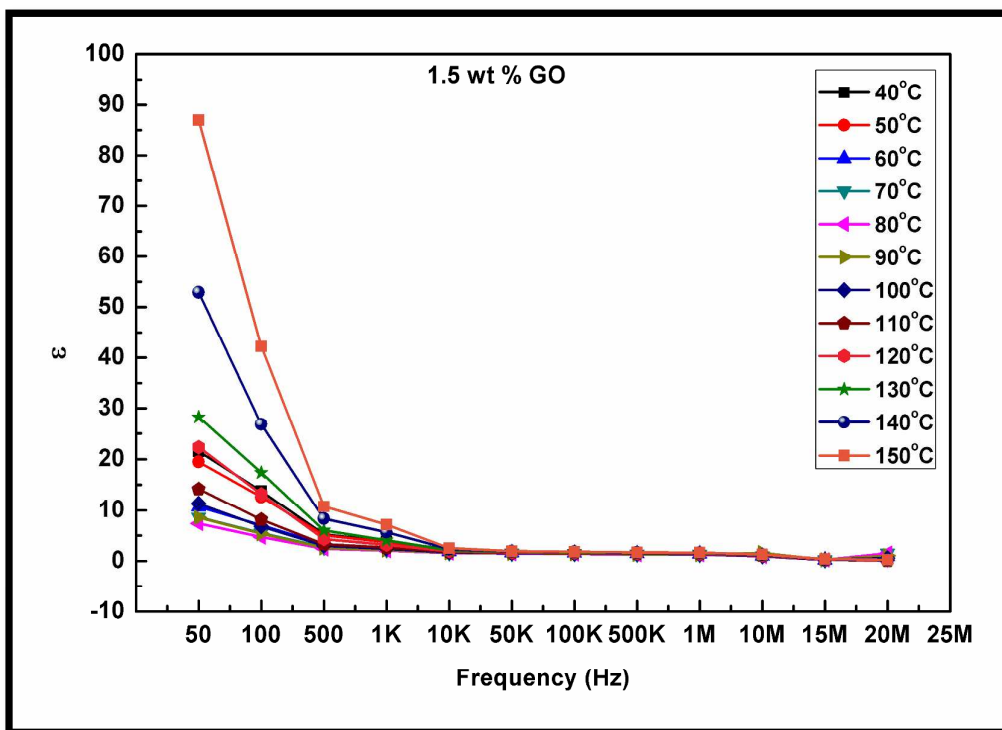


Figure 11 (d): Dielectric constants of WPPy/PVA/GO composite with 1.5 wt% GO loading as a function of frequency at various temperatures.

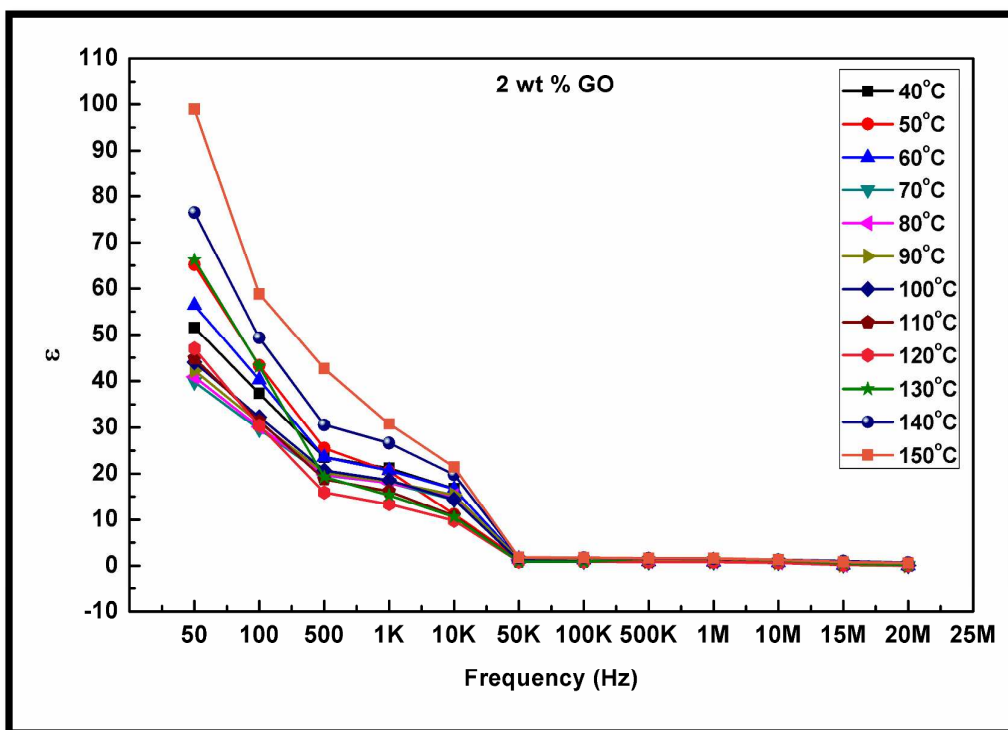


Figure 11 (e): Dielectric constants of WPPy/PVA/GO composite with 2 wt% GO loading as a function of frequency at various temperatures.

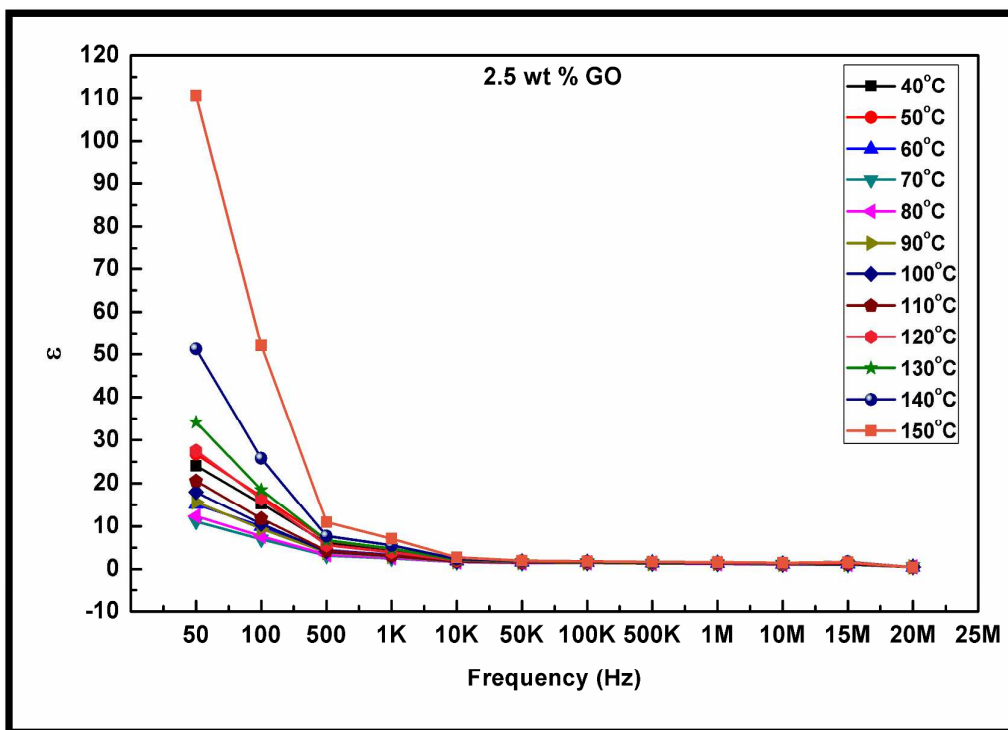


Figure 11 (f): Dielectric constants of WPPy/PVA/GO composite with 2.5 wt% GO loading as a function of frequency at various temperatures.

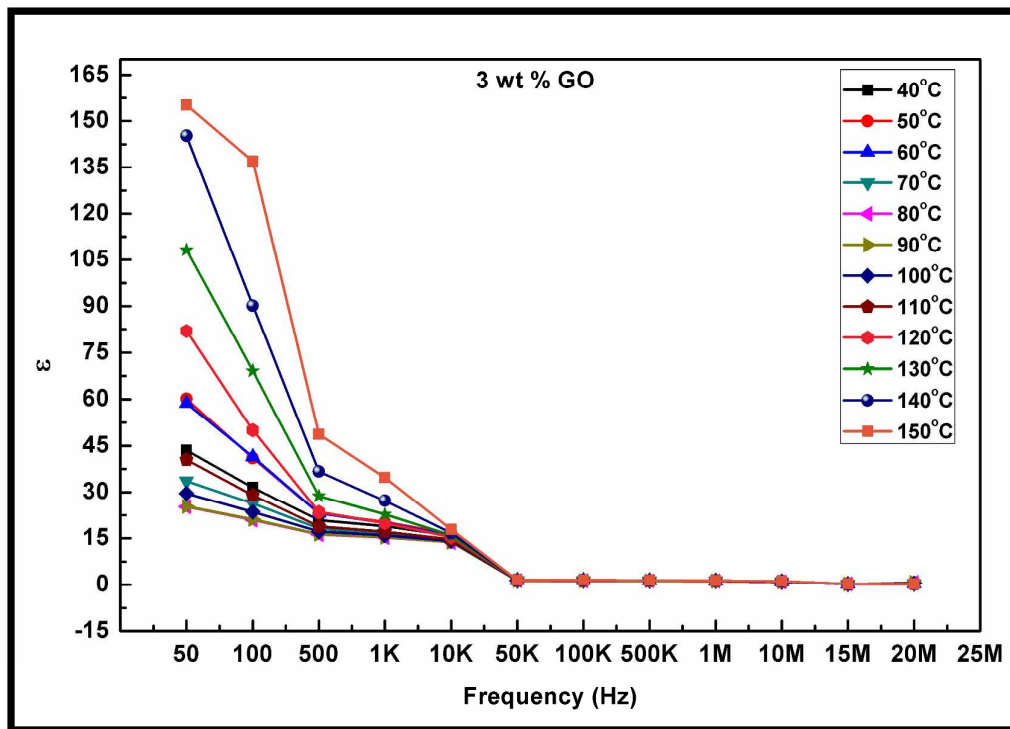


Figure 11 (g): Dielectric constants of WPPy/PVA/GO composite with 3 wt% GO loading as a function of frequency at various temperatures.

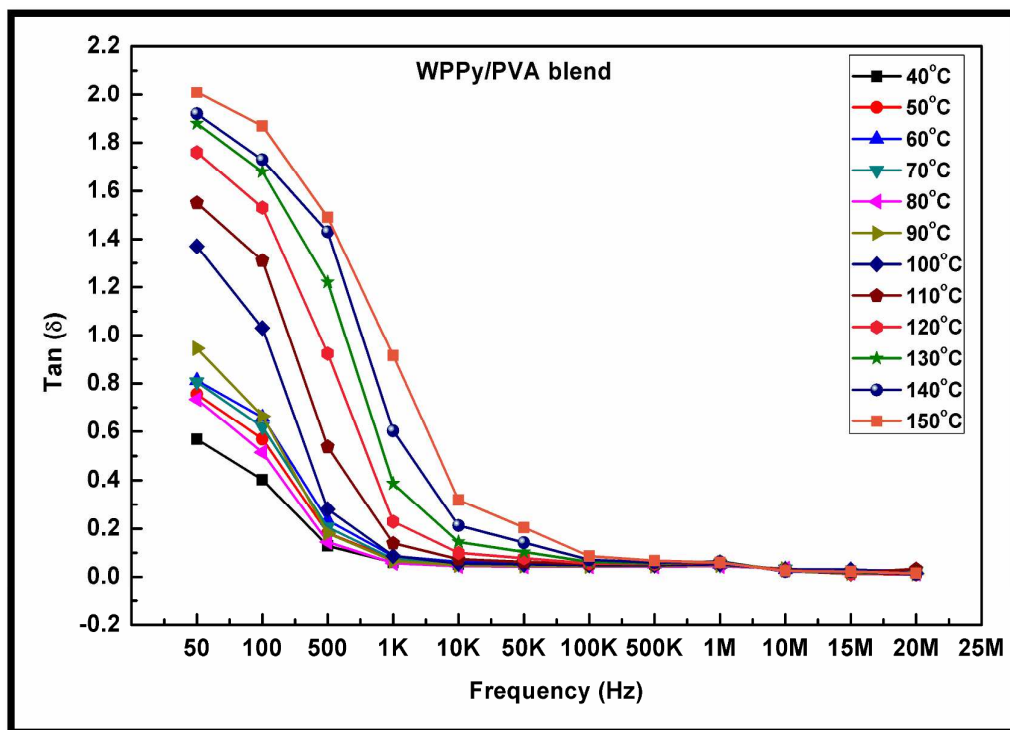


Figure 12 (a): Dielectric loss of WPPy/PVA (50/50) blends as a function of frequency at various temperatures.

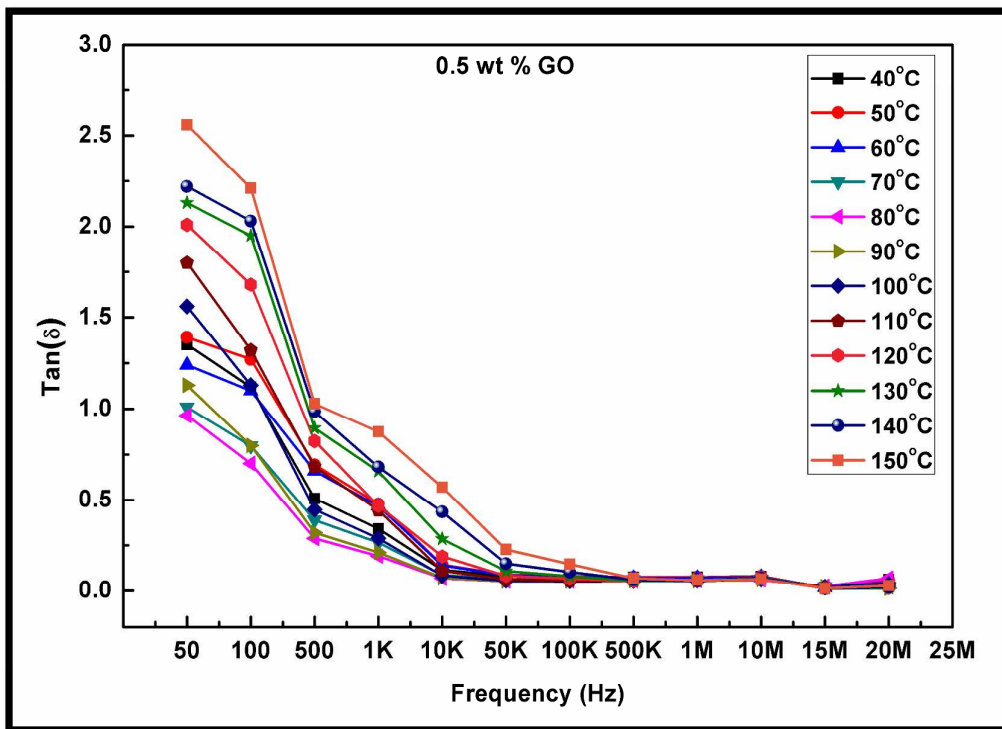


Figure 12 (b): Dielectric loss of WPPy/PVA/GO composite with 0.5 wt% GO loading as a function of frequency at various temperatures.

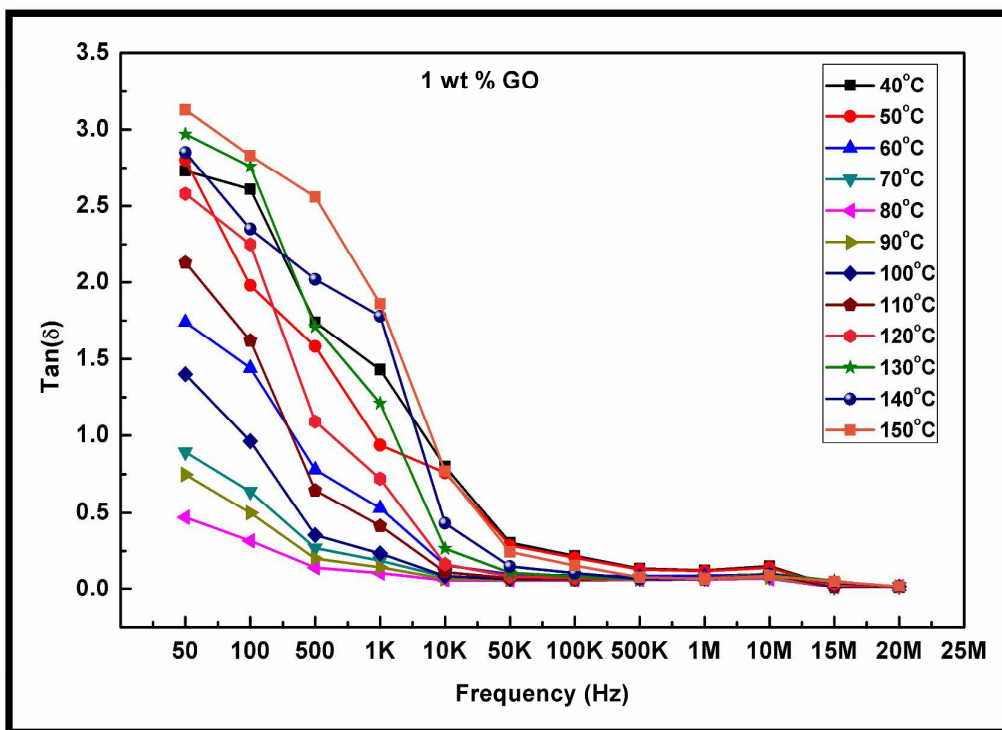


Figure 12 (c): Dielectric loss of WPPy/PVA/GO composite with 1 wt% GO loading as a function of frequency at various temperatures.

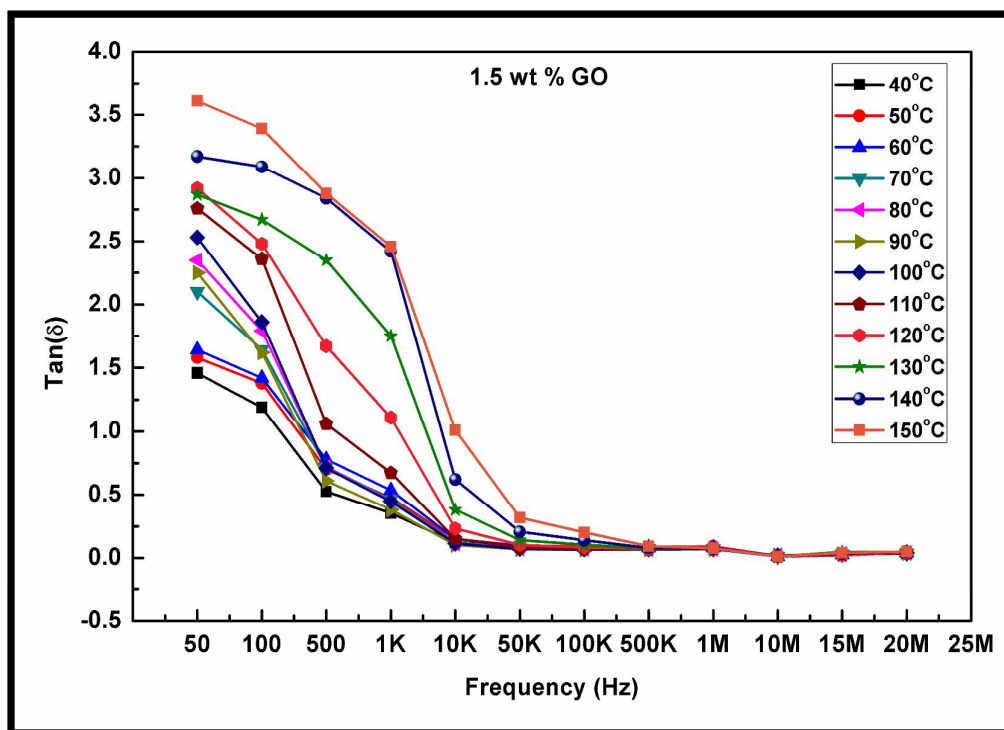


Figure 12 (d): Dielectric loss of WPPy/PVA/GO composite with 1.5 wt% GO loading as a function of frequency at various temperatures.

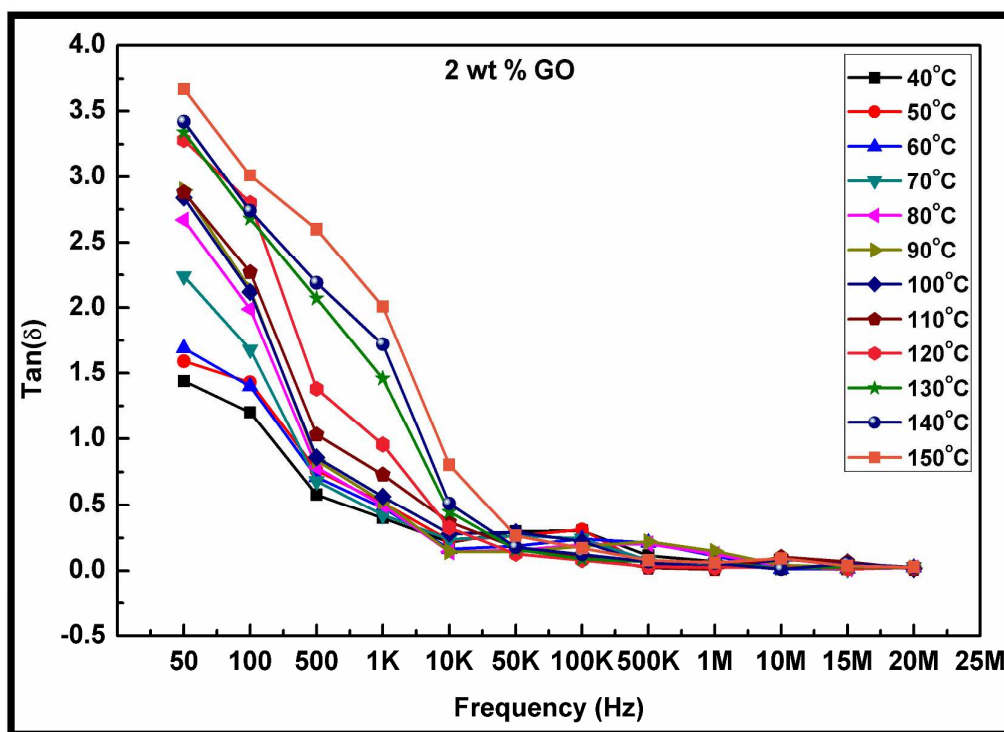


Figure 12 (e): Dielectric loss of WPPy/PVA/GO composite with 2 wt% GO loading as a function of frequency at various temperatures.

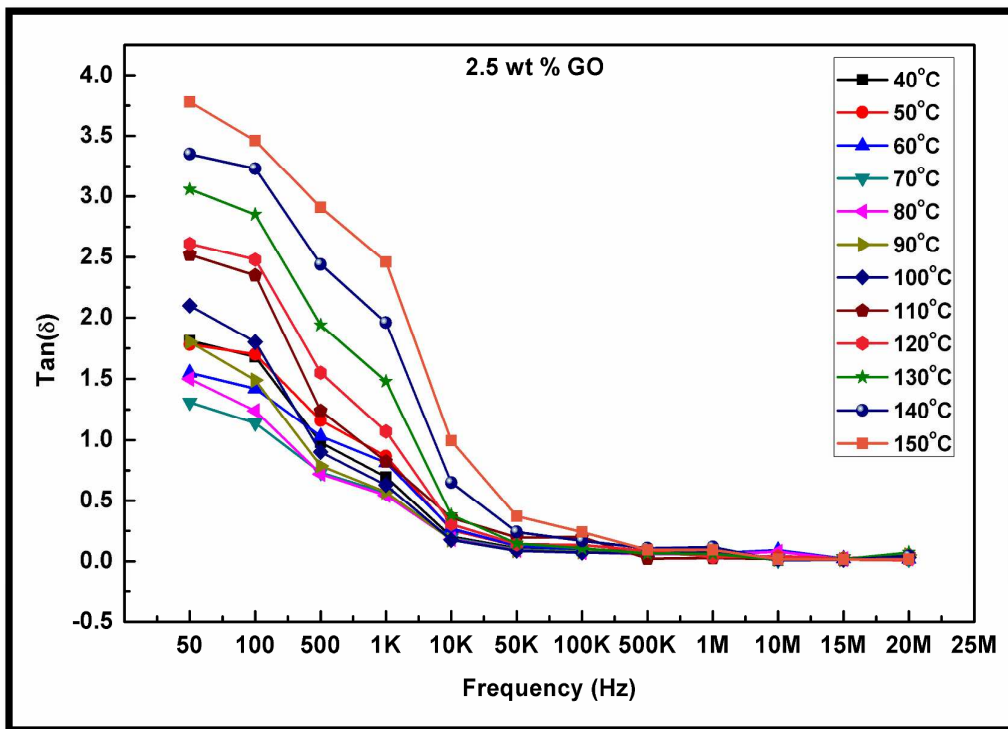


Figure 12 (f): Dielectric loss of WPPy/PVA/GO composites with 2.5 wt% GO loading as a function of frequency at various temperatures.

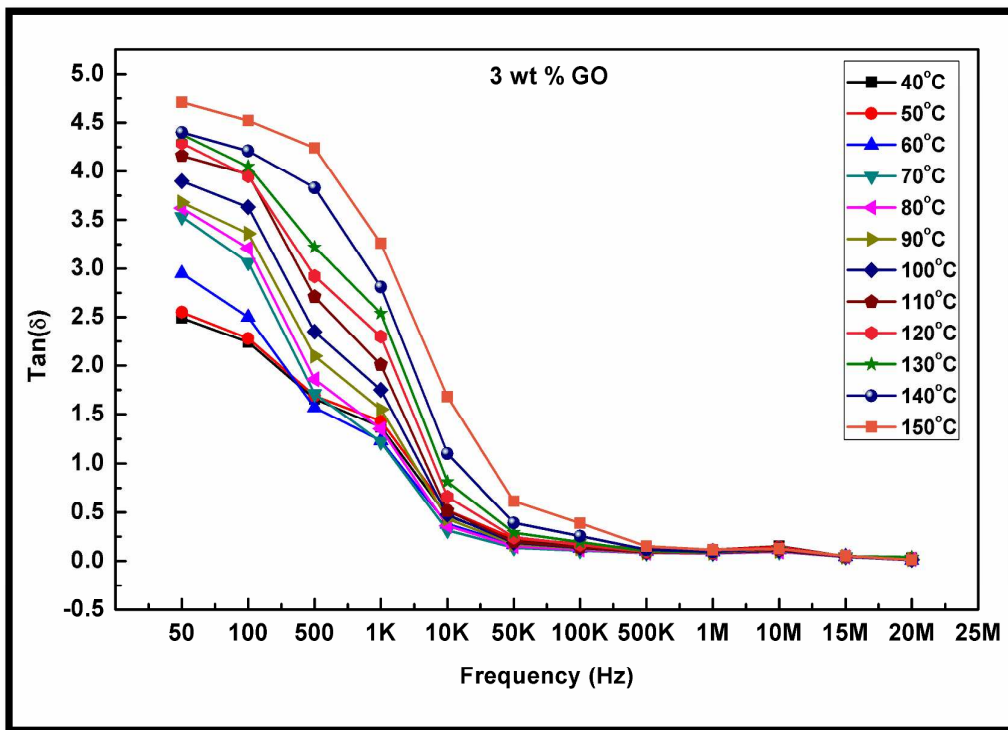


Figure 12 (g): Dielectric loss of WPPy/PVA/GO composites with 3 wt% GO loading as a function of frequency at various temperatures.

Table 1: Feed composition of WPPy/PVA/GO nanocomposites.

WPPy (wt %)	PVA (wt %)	GO (wt %)
50	50	0
49.5	50	0.5
49	50	1
48.5	50	1.5
48	50	2
47.5	50	2.5
47	50	3

Table 2: Maximum values of dielectric constant and dielectric loss obtained for WPPy/PVA/GO nanocomposites with different GO loadings.

GO Loading (wt%)	Dielectric Constant (ϵ)	Dielectric Loss (Tan δ)
0	27.93, 50 Hz, 150°C	2.01, 50 Hz, 150°C
0.5	48.07, 50 Hz, 150°C	2.56, 50 Hz, 150°C
1	75.76, 50 Hz, 150°C	3.13, 50 Hz, 150°C
1.5	86.99, 50 Hz, 150°C	3.61, 50 Hz, 150°C
2	98.96, 50 Hz, 150°C	3.67, 50 Hz, 150°C
2.5	110.56, 50 Hz, 150°C	3.78, 50 Hz, 150°C
3	155.18, 50 Hz, 150°C	4.71, 50 Hz, 150°C

Figure and Table Captions:

Figure 1: Schematic representation of the bonding interaction between WPPy, PVA and GO.

Figure 2(a): Photographs showing WPPy/PVA/GO dispersion having different GO loadings

(a) 0.5 wt % GO (b) 1 wt % GO (c) 1.5 wt % GO (d) 2 wt % GO (e) 2.5 wt % GO
(f) 3 wt % GO

Figure 2(b): Photographs of WPPy/PVA/GO composite films (a) 0.5 wt % GO (b) 1 wt %
GO (c) 2 wt % GO (d) 3 wt % GO loadings

Figure 3: FTIR spectra of WPPy/PVA/GO composite films (a) GO powder (b) PVA (c) 0.5
wt % GO (d) 1 wt % GO (e) 1.5 wt % GO (f) 2 wt % GO (g) 2.5 wt % (h) 3 wt %
GO

Figure 4: Raman spectra of Graphite, GO and WPPy/PVA/GO composite films. (a) Graphite (b) GO (c) 0.5 wt % GO (d) 1.5 wt % GO (e) 2.5 wt % GO (f) 3 wt % GO

Figure 5 (a): UV-vis spectra of PVA, WPPy and GO solution.

Figure 5 (b): UV-vis spectra of WPPy/PVA/GO composites (a) 0.5 wt% GO (b) 1 wt% GO (c) 1.5 wt% GO (d) 2 wt% GO (e) 2.5 wt % GO (f) 3 wt % GO

Figure 6 (a): XRD spectra of (a) Graphite Powder (b) GO Powder (c) PVA

Figure 6 (b): XRD spectra of WPPy/PVA/GO composites (a) 0.5 wt% GO (b) 1 wt% GO (c) 1.5 wt% GO (d) 2 wt% GO (e) 2.5 wt% GO (f) 3 wt % GO

Figure 7(a): TGA thermograms of Graphite and GO powder.

Figure 7(b): TGA thermograms of PVA and WPPy/PVA (50/50) blends.

Figure 7(c): TGA thermograms of WPPy/PVA/GO composites (a) 0.5 wt% GO (b) 1 wt% GO (c) 1.5 wt% GO (d) 2 wt% GO (e) 2.5 wt% GO (f) 3 wt% GO.

Figure 8: Optical microscopy images of WPPy/PVA/GO composites (a) 0.5 wt% GO (b) 1 wt% GO (c) 1.5 wt% GO (d) 2 wt% GO (e) 2.5 wt% GO (f) 3 wt% GO.

Figure 9 (a): SEM micrographs of (a) graphite powder (b) GO powder

Figure 9 (b): SEM micrographs of WPPy/PVA/GO composites (a) 0.5 wt% GO (b) 1 wt% GO (c) 1.5 wt% GO (d) 2 wt% GO (e) 2.5 wt% GO (f) 3 wt% GO.

Figure 10 (a): AFM topographic images of WPPy/PVA/GO composites (a) 0.5 wt% GO (b) 1 wt% GO (c) 1.5 wt% GO (d) 2 wt% GO (e) 2.5 wt% GO (f) 3 wt% GO.

Figure 10 (b): AFM 3D images of WPPy/PVA/GO composites (a) 0.5 wt% GO (b) 1 wt% GO (c) 1.5 wt% GO (d) 2 wt% GO (e) 2.5 wt% GO (f) 3 wt% GO.

Figure 11 (a): Dielectric constants of WPPy/PVA (50/50) blend as a function of frequency at various temperatures.

Figure 11 (b): Dielectric constant of WPPy/PVA/GO composites with 0.5 wt% GO loading as a function of frequency at various temperatures.

Figure 11 (c): Dielectric constants of WPPy/PVA/GO composites with 1 wt% GO loading as a function of frequency at various temperatures.

Figure 11 (d): Dielectric constants of WPPy/PVA/GO composites with 1.5 wt% GO loading as a function of frequency at various temperatures.

Figure 11 (e): Dielectric constants of WPPy/PVA/GO composites with 2 wt% GO loading as a function of frequency at various temperatures.

Figure 11 (f): Dielectric constants of WPPy/PVA/GO composites with 2.5 wt% GO loading as a function of frequency at various temperatures.

Figure 11 (g): Dielectric constants of WPPy/PVA/GO composites with 3 wt% GO loading as a function of frequency at various temperatures.

Figure 12 (a): Dielectric loss of WPPy/PVA (50/50) blends as a function of frequency at various temperatures.

Figure 12 (b): Dielectric loss of WPPy/PVA/GO composites with 0.5 wt% GO loading as a function of frequency at various temperatures.

Figure 12 (c): Dielectric loss of WPPy/PVA/GO composites with 1 wt% GO loading as a function of frequency at various temperatures.

Figure 12 (d): Dielectric loss of WPPy/PVA/GO composites with 1.5 wt% GO loading as a function of frequency at various temperatures.

Figure 12 (e): Dielectric loss of WPPy/PVA/GO composites with 2 wt% GO loading as a function of frequency at various temperatures.

Figure 12 (f): Dielectric loss of WPPy/PVA/GO composites with 2.5 wt% GO loading as a function of frequency at various temperatures.

Figure 12 (g): Dielectric loss of WPPy/PVA/GO composites with 3 wt% GO loading as a function of frequency at various temperatures.

Table 1: Feed composition of WPPy/PVA/GO nanocomposites.

Table 2: Comparative values of dielectric constant and dielectric loss of nanocomposites as a function of nanofiller loadings.